Published online 20 January 2023

Nucleic Acids Research, 2023, Vol. 51, No. 4 ***1823–1842***
https://doi.org/10.1093/nar/gkac1275

Cold-induced inhibition of photosynthesis-related genes integrated by a TOP6 complex in rice mesophyll cells

Zhan Xu[1,*,†], Jianxiang Zhang[2,†], Xu Wang[3,†], Jemaa Essemine[4], Jing Jin[4], Mingnan Qu[5,*], Yong Xiang[3,*] and Weixiong Chen[1,*]

[1]Guangzhou City Academy of Agricultural Sciences, Key Laboratory of Biology, Genetics and Breeding, Pazhou Dadao Rd 17-19, Haizhu District, Guangzhou 510000, China, [2]Key Laboratory of Plant Functional Genomics of Ministry of Education/Jiangsu Key Laboratory of Crop Genetics, Yangzhou University, Yangzhou 225009, China, [3]Shenzhen Branch, Guangdong Laboratory of Lingnan Modern Agriculture, Genome Analysis Laboratory of the Ministry of Agriculture and Rural Affairs, Agricultural Genomics Institute at Shenzhen, Chinese Academy of Agricultural Sciences, Shenzhen 518000, China, [4]Laboratory of Photosynthesis and Environment, CAS Center for Excellence in Molecular Plant Sciences, Shanghai Institute of Plant Physiology and Ecology, Chinese Academy of Sciences, Shanghai 200032, China and [5]Hainan Yazhou Bay Seed Laboratory, Sanya 572025, China

Received August 13, 2022; Revised December 18, 2022; Editorial Decision December 21, 2022; Accepted December 25, 2022

ABSTRACT

Photosynthesis is the most temperature-sensitive process in the plant kingdom, but how the photosynthetic pathway responds during low-temperature exposure remains unclear. Herein, cold stress (4°C) induced widespread damage in the form DNA double-stranded breaks (DSBs) in the mesophyll cells of rice (*Oryza sativa*), subsequently causing a global inhibition of photosynthetic carbon metabolism (PCM) gene expression. Topoisomerase genes *TOP6A3* and *TOP6B* were induced at 4°C and their encoded proteins formed a complex in the nucleus. TOP6A3 directly interacted with KU70 to inhibit its binding to cold-induced DSBs, which was facilitated by TOP6B, finally blocking the loading of LIG4, a component of the classic non-homologous end joining (c-NHEJ) pathway. The repression of c-NHEJ repair imposed by cold extended DSB damage signaling, thus prolonging the inhibition of photosynthesis in leaves. Furthermore, the TOP6 complex negatively regulated 13 crucial PCM genes by directly binding to their proximal promoter regions. Phenotypically, *TOP6A3* overexpression exacerbated the γ-irradiation-triggered suppression of PCM genes and led to the hypersensitivity of photosynthesis parameters to cold stress, dependent on the DSB signal transducer ATM. Globally, the TOP6 complex acts as a signal integrator to control PCM gene expression and synchronize cold-induced photosynthesis inhibition, which modulates carbon assimilation rates immediately in response to changes in ambient temperature.

INTRODUCTION

Climate change is raising the intensity, frequency and duration of abnormal weather events, which include periods of unseasonably cold and warm temperatures (1,2). Low temperature can be classified as cold (0–15°C) or freezing (<0°C) stress, which are the most severe weather events limiting crop growth, productivity and geographical distribution (3). Rice (*Oryza sativa* L.) is a thermophilic cereal crop originating from tropical and subtropical regions that is highly susceptible to cold stress, in contrast to other cereal crops such as wheat (*Triticum aestivum* L.) and barley (*Hordeum vulgare* L.) which are more resilient to cold temperatures (4).

Plants capture solar energy and assimilate carbon dioxide (CO_2) through photosynthesis, which represents the primary component modulating crop yield and is the most temperature-sensitive target machinery. Most plants possess a considerable capacity to adjust their photosynthetic characteristics in response to fluctuating ambient temperatures (5,6). Physiological photosynthesis can be suppressed

*To whom correspondence should be addressed. Email: xuzhan@sippe.ac.cn
Correspondence may also be addressed to Mingnan Qu. Email: qmn@yazhoulab.com
Correspondence may also be addressed to Yong Xiang. Email: xiangyong@caas.cn
Correspondence may also be addressed to Weixiong Chen. Email: cgchen@sibs.ac.cn
†The authors wish it to be known that, in their opinion, the first three authors should be regarded as Joint First Authors.

under both low and high temperatures (7). In particular, cold stress impairs the chloroplast microstructure, photosynthetic metabolism and energy production, which is accompanied by oxidative damage and a disruption of cell membrane integrity (8–10).

In response to changes in their local environment, plants undergo a coordinated modulation in the expression of genes encoding different components of the photosynthetic machinery. For instance, both salt and drought stresses down-regulate some photosynthetic genes, although salt stress affects the expression of far more genes than drought stress (11). Under a combination of drought stress and high temperature, the transcription factor (TF) HIGHER YIELD RICE (HYR) was shown to directly activate its downstream target genes and up-regulate genes from the photosynthetic carbon metabolism (PCM) pathway in rice (12). Cold stress disrupts the proper functioning of the systems that regulate photosynthesis (13) and causes the transcriptional repression of genes associated with chlorophyll biosynthesis and chloroplast development (14,15). However, the molecular mechanism underlying this phenomenon remains unknown.

DNA topoisomerase (Top) activity has previously been reported to be implicated in DNA templating processes, such as transcription (16–18), DNA replication (16,19) and DNA repair (20,21). Top6 from Archaea consists of two distinct subunits, Top6A and Top6B. Top6A is the catalytic subunit and is responsible for DNA binding and cleavage, while Top6B is involved in ATP binding and hydrolysis (22,23). The eukaryotic homolog of archaeal Top6A is SPORULATION 11 (SPO11), which can induce meiosis-specific double-stranded breaks (DSBs) by a TOP II-like mechanism (24,25). In the model plant Arabidopsis (*Arabidopsis thaliana*), Top6 homologs appear to function in two discrete processes: AtSPO11-1 and AtSPO11-2 participate in meiotic recombination, while AtSPO11-3 contributes to somatic DNA replication (26). Another report showed that the Arabidopsis TOP6 complex (comprising AtSPO11-3 and AtTOP6B) appears to be essential for endoreduplication in somatic cells (27). Moreover, the AtTOP6 complex plays key regulatory roles in the signaling pathways of brassinosteroids (28), auxin (29) and reactive oxygen species (ROS) (30).

Here, we demonstrate that cold treatment at 4°C induces massive DSB damage in the nucleus of rice mesophyll cells (MCs), which subsequently activates the master regulator DSB transducer ATAXIA-TELANGIECTASIA MUTATED (ATM), thereby causing a significant transcriptional inhibition of global PCM genes, including genes encoding chlorophyll (Chl) *a,b*-binding proteins, light-harvesting complexes (LHCs), subunits of the photosystem II (PSII) and PSI reaction centers (RCs), chloroplast ATP synthase subunits, electron transport reaction components and enzymes from the Calvin–Benson–Bassham (CBB) cycle. We therefore propose that cold stress induces a DSB damage response that transcriptionally represses photosynthetic genes by activating the ATM kinase in rice MCs.

We also characterized the roles of the rice TOP6 complex (TOP6A3 and TOP6B) in integrating cold-inhibited PCM gene expression, which comprises two distinct regulatory functions: (i) TOP6A3 negatively regulates PCM genes (*Lhca2*, *Lhcb1.1*, *Lhcb1a*, *Lhcb2.1*, *Lhcb6*, *PORA*, *HEMB*, *HEMA*, *PsaN*, *PsaO*, *PsbR1*, *PsbQ* and *RbcS1*) by directly binding to proximal promoter regions, which is a prerequisite for their inhibition during the cold response; and (ii) TOP6A3 interacts with KU70, the first step protein in the c-NHEJ pathway, and inhibits its binding to cold-induced DSBs. This process is promoted by TOP6B and leads to the attenuation of ligase4 (LIG4) loading in the KU-mediated repair pathway, which extends the DSB damage signal and prolongs the transcriptional inhibition of PCM genes under cold stress.

MATERIALS AND METHODS

Plant materials and growth conditions

Mutant rice lines (*ku70*, *lig4*, *atm-1* and *atr*) reported in our previous studies (31,32) were used. The clustered regularly interspaced short palindromic repeat (CRISPR)/CRISPR-associated nuclease 9 (Cas9)-induced mutants (*top6a3*, *top6b* and *atm-2*) were created using a modified method based on the basic CRISPR/Cas9 system (33). Two steps were used for constructing the CRISPR/Cas9 vectors, involving an intermediate vector (SK-gRNA) and a final vector (pC1300-Cas9). To generate transgenic rice plants overexpressing *TOP6A3* and *TOP6B*, their coding sequences were individually amplified from first-strand cDNA. The resulting polymerase chain reaction (PCR) products were then separately cloned into the pCAMBIA1300 vector, which harbors the cauliflower mosaic virus (CaMV) 35S promoter. The constructs were thereafter transformed into the rice *japonica* variety Kangtiao 3 (K3). Homozygous lines of the T_3 generation (*TOP6A3-OE1* and *TOP6B-OE1*) were used for analysis. The double overexpressing line (*TOP6A3-OE1 TOP6B-OE1*) was obtained by crossing *TOP6A3-OE1* and *TOP6B-OE1* plants; similarly, the *TOP6A3-OE1 atm* line was obtained by crossing a *TOP6A3-OE1* plant with the *atm-2* mutant. All plant materials used in this study were grown in paddy fields under normal conditions. Genomic DNA extraction was performed with a Tissuelyser-48 instrument (Jingxin Technology). The complete information on all rice lines is provided in Supplementary Table S2 and the primers used for genotyping are given in Supplementary Table S3.

Measurements of leaf photosynthesis levels and physiological parameters

Seeds were sown on May 30 at a Shanghai field base. For each genotype, 36 individuals were planted (6 × 6) with 20 cm between rows and 15 cm between plants of the same row. The rice fields were managed according to standard local agronomic practice as described previously (34). The recorded mean air temperature from the sowing date until the photosynthetic measurements was ∼24.8°C (±3.1°C).

The middle section of fully expanded leaves from each plant was used for photosynthetic measurements. The experiments were conducted between 9:00 am and 11:30 am using a portable photosynthesis system (Li-COR Inc., Lincoln, NE, USA). The temperature and CO_2 concentration in the cuvette chamber were maintained at 25°C (or 8°C) and 400 ppm, respectively. A light intensity of 1000 μmol

m^{-2} s^{-1} was used to assess the photosynthetic rates under saturated light conditions (A_{sat}). Four biological replicates were performed for each genotype.

For the chilling stress treatment, rice plants were moved indoors and exposed to 4°C for 24 h. During the measurement of photosynthetic parameters, the temperature and CO_2 concentration in the cuvette chamber were maintained at 4°C and 400 ppm, respectively.

Gene expression analysis

For transcriptome deep sequencing (RNA-seq), the total RNA was isolated from the leaf tissue of 14-day-old mutants (*top6a3*, *atm-1* and *atr*), the overexpressing line (*TOP6A3-OE1*), the *TOP6A3-OE1 atm* plant and wild-type (WT) plants (*ATM* and K3) using an RNA extraction kit (Huayueyang, China). RNA integrity was checked on 1% (w/v) agarose gels and on a NanoPhotometer spectrophotometer (IMPLEN, CA, USA). Total RNA concentration was measured by a Qubit RNA Assay Kit on a Qubit 2.0 Flurometer (Life Technologies, CA, USA), and RNA integrity was evaluated using an RNA Nano 6000 Assay Kit on a Bioanalyzer 2100 system (Agilent Technologies, CA, USA). The construction of RNA-seq libraries was performed using a NEBNext Ultra Directional RNA Library Prep Kit for Illumina (NEB, Ipswich, MA, USA) following the manufacturer's instructions. The RNA-seq libraries were sequenced on an Illumina HiSeq-2000 instrument as 100 bp single-end reads. Library sequencing was performed by PANOMIX Biomedical Tech Co., Ltd (Suzhou, China).

For reverse transcription–quantitative PCR (RT–qPCR) analysis, total RNA was extracted from rice leaves tissues using a Trelief® RNApre Pure Plant Kit (singke, code: TSP411) according to the manufacturer's instructions. The RNA samples without any genomic DNA were reverse transcribed to first-strand cDNA using a Goldenstar® RT6 cDNA Synthesis Kit (singke, code: TSK301S). qPCR was performed in a total volume of 20 μl using 2 μl of cDNA as template with 0.6 μl of each reverse and forward primer (R + F, 10 μM) and 10 μl of 2× TSINGKE® Master qPCR Mix (code: TSE201) on a Qtower 3.0 real-time PCR instrument (Analytik Jena, Germany), then the total volume was adjusted to 20 μl by adding 6.8 μl of water. Fluorescence was quantified against standards. The PCR conditions were as follows: 5 min at 95°C, followed by 41 cycles at 95°C for 10 s, 52°C for 30 s and 72°C for 30 s. Melting temperatures (MTs) were determined for each gene product. *UBQ* (Os03g0234200) was used as an internal control (housekeeping gene) for normalization of expression levels in rice. Relative expression levels were evaluated based on the $2^{-\Delta\Delta CT}$ method, as described by Livak and Schmittgen (35). For each gene, three biological replicates were performed. The sequences of the qRT-PCR primers are given in Supplementary Table S3. All chemicals for RT–qPCR analysis were purchased from singke Biotechnology Co., Ltd (China).

Antibody production

The anti-TOP6A3 antibody was produced by Orizymes Biotechnology (Shanghai) Co. Ltd. Briefly, a TOP6A3 peptide fragment (Supplementary Table S1) was used to produce a specific antibody by immunizing one rabbit with the fusion peptides. Vector construction, production of the fusion peptide and protein purification were performed as previously described (36). An immunoblot assay was conducted to confirm that the prepared anti-TOP6A3 antibody was specific for TOP6A3 in rice (Supplementary Figure S2C). The other antibodies against RAD51C, RAD51, XRCC3, COM1, LIG4 and γ-H2AX used in this study were as reported in our previous studies (31,37). Detailed information about all the antibodies is provided in Supplementary Table S4.

Yeast two-hybrid (Y2H) assay, pull-down assay and electrophoretic mobility shift assay (EMSA)

For Y2H assays, the coding sequences of the relevant genes were amplified and cloned individually into the pGADT7 and pGBKT7 vectors. The appropriate pairs of constructs were transformed into yeast strain Y2HGOLD, and positive colonies were selected on synthetic defined (SD) medium lacking Leu and Trp (SD –Leu –Trp). Protein–protein interactions were tested by growth on SD medium lacking Leu, Trp, His and Ade (SD –Leu –Trp –His –Ade). Primers used for the cloning of Y2H constructs are listed in Supplementary Table S3.

For pull-down assays, recombinant purified glutathione *S*-transferase (GST) fusion proteins (GST–TOP6A3, GST–TOP6B and the negative control GST) were incubated with glutathione Sepharose 4B (GE Healthcare) in pull-down buffer [50 mM Tris–HCl, pH 8.0, 150 mM NaCl, 10% (v/v) glycerol, 0.5 mM EDTA, 0.1% (v/v) Triton X-100, 5 mM 2-mercaptoethanol and protease inhibitor cocktail] for 4 h at 4°C, and then recombinant KU70-HIS was added and incubated for another 3 h at 4°C. After washing five times with pull-down buffer, Sepharose beads were collected by brief centrifugation (2000 *g*, 3 min) and then resuspended in protein extraction buffer. Proteins were separated by sodium dodecylsulfate (SDS)–polyacrylamide gel electophoresis (PAGE) and detected by immunoblot analysis with the appropriate antibodies.

For EMSAs, 20 fmol of labeled probe was incubated in binding buffer, 2.5% (v/v) glycerol, 50 mM KCl, 5 mM $MgCl_2$ and 10 mM EDTA with or without recombinant proteins at 28°C for 20 min. Pull-down assays and EMSAs were performed by Nanjing bayico Biotechnology Co., Ltd (Nanjing, China).

Firefly luciferase complementation imaging (LCI) assay

The coding sequences of *KU70* and *TOP6* (*TOP6A3* and *TOP6B*) were cloned into the pCAMBIA1300-nLUC and pCAMBIA1300-cLUC vectors, respectively. Agrobacterium (*Agrobacterium tumefaciens*) strain GV3101 carrying the indicated constructs was cultured to an OD_{600} of 0.5 in Luria–Bertani (LB) medium and incubated at room temperature without shaking for 3 h. The cell suspensions were then infiltrated into *Nicotiana benthamiana* leaves (38). Luciferase activity was detected 2 days after infiltration with an LB 985 NightSHADE system (Berthold Technologies).

Chromatin immunoprecipitation (ChIP)

The ChIP assay was performed as previously described (39). Briefly, rice leaf samples (5 g) were cross-linked in buffer containing 4% (w/v) formaldehyde. Nuclei were isolated and chromatin was sheared by sonication into 200–600 bp fragments. Sonicated chromatin was pre-cleared with 100 μl of protein A–agarose for 1.5 h and immunoprecipitated into two fractions: one fraction with anti-TOP6A3 for TOP6A3-bound chromatin and one fraction with anti-histone H3 (AHO1432, Invitrogen, 1.5–2 mg) as a non-specific chromatin-binding protein. Chromatin-bound DNA fragments were eluted after reverse cross-linking by incubation overnight with proteinase K at 37°C. The incubation was repeated at 65°C overnight and subsequently the DNA was purified following the manufacturer's instructions. ChIP assays were performed based on three biological replicates, and qPCR analysis was carried out in triplicate with primers designed to amplify putative TOP6A3-bound promoters for each ChIP assay (Supplementary Table S3).

TOP6A3 and TOP6B subcellular localization

The coding sequences of *TOP6* genes (*TOP6A3* or *TOP6B*) were cloned into the pJIT163-GFP vector in-frame with the sequence of green fluorescent protein (*GFP*). The coding sequence of *OsbZIP52* was cloned into the pSAT6-RFP vector in-frame with the sequence of red fluorescent protein (*RFP*). The appropriate pairs of plasmids were co-transfected into rice protoplasts. After incubation in the dark at 28°C for 20 h, fluorescence signals were observed using a confocal laser scanning microscope (Carl Zeiss LSM 710). GFP and RFP were excited at 488 nm and 561 nm, and their signals were observed at 500–540 nm and 600–650 nm, respectively. *OsbZIP52-RFP* was used as a nuclear localization marker (40).

Immunofluorescence staining of MCs, root tips and protoplasts

For immunostaining of MCs, samples were collected from mutants (*top6a3* and *top6b*), the double overexpressing line (*TOP6A3-OE1 TOP6B-OE1*) and their WT following cold treatment at 4°C for 24 h. MCs were isolated from rice leaves, fixed in 4% (w/v) paraformaldehyde at 4°C for 30 min and then stored at –80°C in 10% (v/v) phosphate-buffered saline (PBS). For immunostaining of root tips, seedlings from the mutants and their WT siblings were harvested following irradiation with ^{60}Co γ-ray (40 Gy). After 20 min of recovery from irradiation, root tips were collected and fixed in 4% (w/v) paraformaldehyde at 4°C for 30 min and then stored at –80°C in 10% (v/v) PBS. For immunostaining of protoplasts, transformed calli with the T-DNA of pI-SceI.CON, which was selected on hygromycin for 20 days, were used to prepare protoplasts. The coding sequence of *TOP6A3* was cloned into the pJIT163-GFP vector, and the I-SceI gene (Supplementary Table S5, encoding an endonuclease with restriction site TAGGGATAACAGGGTAAT) was cloned into the pSAT6-RFP vector. The two plasmids were then co-transfected into rice protoplasts. After incubation in the dark at 28°C for 20 h, the rice protoplasts were collected and fixed in 4% (w/v) paraformaldehyde at 4°C for 20 min.

The procedures of slide preparation and immunodetection were as previously described (41). The nuclei were counter-stained with Vector-shield mounting medium containing 4′,6-diamidino-2-phenylindole (DAPI; Vector Laboratory, cat. no. H-1200), and the specific immunosignals were captured as digital images using a fluorescence microscope (Olympus DP80). For the root tips, interphase nuclei were selected for photographs and quantitative analyses.

Comet assay

Leaf tissues from control and cold-treated rice seedlings for the mutants (*top6a3* and *top6b*), the double overexpressing line (*TOP6A3-OE1 TOP6B-OE1*) and their WT (K3) siblings, were used for preparation of nuclei. A single-cell gel electrophoresis assay (Comet) for DSB detection was performed with a commercial kit (CTCC-M001) as described previously (42,43). Nuclear lysis was performed at 4°C for 1 h instead of at room temperature for 20 min. After staining with propidium iodide (PI; Sigma, cat. no. p4170), comet images were captured using a fluorescent microscope (Olympus DP80) equipped with a CCD camera. DNA damage signals were analyzed using the comet assay software project (CASP) software. Thirty typical nuclei were selected for statistical analysis, and each measurement was performed three times. All chemicals for the comet assay were purchased from CTCC (Wuxi, China).

RESULTS

Cold-induced *TOP6* genes (*TOP6A3* and *TOP6B*) in rice and their negative regulatory roles in chlorophyll (Chl) biosynthesis

To clarify the potential functions of *TOP6* genes, we measured their transcript levels in response to certain abiotic stresses by RT–qPCR. We determined that *TOP6A3* and *TOP6B* are strongly up-regulated following cold treatment (4°C), but not following exposure to 12°C or to other abiotic stresses, including osmotic stress, dehydration, DNA damage, high salinity or heat stress (42°C) (Figure 1A). We also raised a specific polyclonal antibody against rice TOP6A3 (Supplementary Table S1). We observed an accumulation of TOP6A3 by immunoblot analysis in both cold-treated roots and leaves (Figure 1B).

In Arabidopsis, mutation in either AtTOP6B or AtSPO11-3 causes severe dwarfing (26,44), but the plants remain fully capable of forming all plant tissues as in the WT. In this report, we obtained rice mutants (*top6a3* and *top6b*) via CRISPR/Cas9-mediated gene editing (Figure 1C). Both single mutants exhibited clear growth retardation from 12 to 24 days post-germination (Figure 1D, E), and their leaves took on a dark-green appearance (Figure 1F). Notably, Chl *a* accumulated to higher levels in the mutants, with a 2.5- and 2.8-fold increase in *top6a3* and *top6b*, respectively, relative to the WT. Likewise, Chl *b* contents also increased by 90% and 80% in the *top6a3* and *top6b* mutants, respectively, relative to the WT (Figure 1G; Supplementary Data S1).

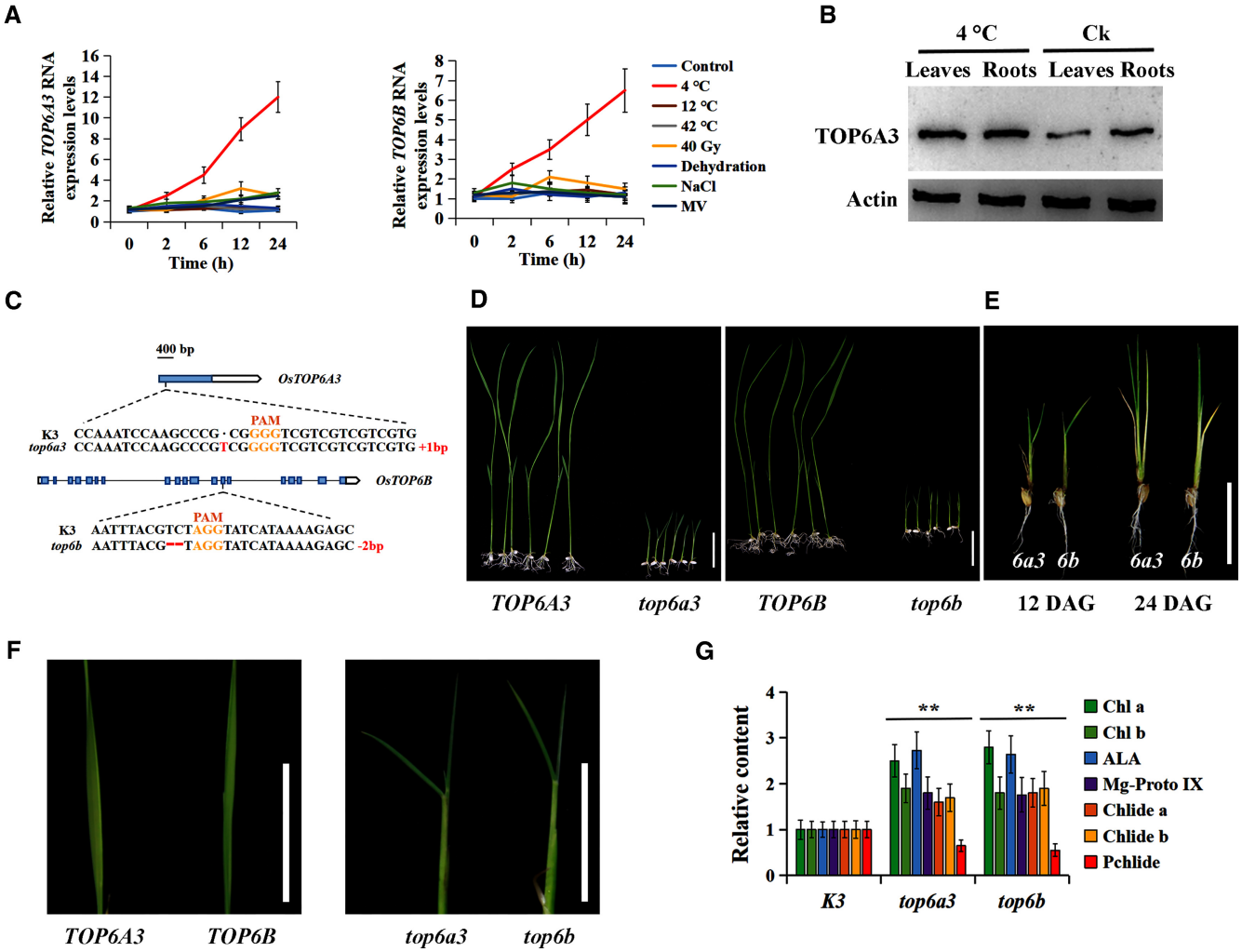

Figure 1. Relative expression levels of *TOP6* genes and Chl biosynthesis phenotypes of the *top6a3* and *top6b* mutants. (**A**) RT–qPCR analysis of *TOP6A3* and *TOP6B* expression levels in response to various abiotic stress conditions. Total RNA samples were extracted from the leaves of 2-week-old WT seedlings at the given time points after exposure to cold (4°C), heat (42°C), γ-irradiation (40 Gy), 25% (w/v) polyethylene glycol (PEG), salt (250 mM NaCl) or methyl viologen (10 μM MV). Rice *UBQ* was used for normalization. Experiments were performed three times. Data are means ± standard error (SE, $n = 6$). (**B**) Immunoblot analysis for TOP6A3 abundance in rice leaves and roots 24 h after cold treatment. Actin served as the loading control. The immunoblot assay was repeated twice, yielding identical results. (**C**) Schematic diagrams of the *TOP6A3* and *TOP6B* loci. Coding regions are shown as blue boxes; 5′- and 3′-untranslated regions are shown in white boxes; introns are shown as black lines. The red nucleotides or dashes indicate the mutation sites induced by CRISPR/Cas9-mediated editing. (**D–F**) Representative phenotypes of *top6a3* and *top6b* mutants and WT plants. Scale bars, 3 cm (D, E), 2 cm (F). *6a3*, *top6a3*; *6b*, *top6b*. (**G**) Contents of Chl biosynthesis intermediates (Chl *a*, Chl *b*, ALA, Mg-protoIX, Chlide *a*, Chlide *b and* Chlide) in the leaves of *top6a3* and *top6b* mutants and K3.

To explore how Chl accumulated to higher levels in the mutants, we measured the levels of metabolic intermediates of the Chl biosynthetic pathway. δ-Aminolevulinic acid (ALA) represents the first intermediate of Chl biosynthesis and reached levels 2.7- and 2.6-fold higher in the *top6a3* and *top6b* mutants, respectively, compared with the WT (Figure 1G; Supplementary Data S1). Mg-protoIX constitutes the first intermediate of the magnesium (Mg) branch of the Chl biosynthesis pathway, and its levels were 80% and 76% higher in the *top6a3* and *top6b* mutants, respectively, relative to the WT. Pchlide can be converted to chlorophyllide (Chlide) by protochlorophyllide oxidoreductase (POR) in a light-dependent manner (45). In this study, we observed that the Pchlide content is drastically decreased in the mutants, while Chlide *a* and Chlide *b* levels were ∼2-fold higher in the mutants compared with the WT. We conclude that mutation of *TOP6* genes promoted the conversion of Pchlide to Chlide in rice leaves.

We also overexpressed *TOP6A3* or *TOP6B* individually in WT [variety Kangtiao 3 (K3)] plants to test their biological functions; two representative transgenic lines (*TOP6A3-OE1* and *TOP6B-OE1*) were selected for further investigation (Supplementary Figure S1A, B). Notably, *TOP6A3-OE1* plants showed a 35.3-fold increase in relative *TOP6A3* transcript levels, while *TOP6B-OE1* plants displayed a 28.1-fold increase in *TOP6B* expression compared with K3 plants (Supplementary Figure S1D). Importantly, we did not observe significant differences in plant architecture between the WT and the overexpressing lines, although *TOP6A3-OE1* plants were slightly shorter than the WT at

the reproductive stage (Supplementary Figure S1B, E), with a slight acceleration of heading time in *TOP6A3-OE1* relative to K3 (Supplementary Figure S1C, F). Furthermore, we generated the double overexpressing line *TOP6A3-OE1 TOP6B-OE1* by crossing the *TOP6A3-OE1* and *TOP6B-OE1* lines (Supplementary Figure S1G, I). Again, we did not detect significant differences in terms of Chl contents or expression of Chl biosynthetic genes during the early seedling stage in the double overexpressing line compared with K3 seedlings (Supplementary Figure S1J, L). Notably, we observed that de-etiolation is slower, and Chl (Chl *a* and Chl *b*) accumulation was significantly lower in the double overexpressing line relative to K3 seedlings following the transfer of etiolated seedlings to light for 24 h (Supplementary Figure S1H, K; Supplementary Data S2).

Together, these results indicate that *TOP6* genes might be involved in the response to cold stress. The phenotypes associated with loss-of-function mutants and overexpression lines reveal that *TOPA3* and *TOP6B* play negative regulatory roles in Chl biosynthesis, probably by repressing ALA biosynthesis and the conversion of Pchlide into Chlide in rice leaves.

The TOP6 complex negatively regulates 13 crucial PCM genes by directly binding to the proximal promoter region

To better delineate the negative effects exerted by the TOP6 complex on Chl biosynthesis, we carried out RNA-seq analysis of rice leaves from the *top6a3* mutant and K3 seedlings. Following the identification of differentially expressed genes (DEGs) between the mutant and the WT, as illustrated by heatmaps and volcano plots (Figure 2A, B), we defined a group of up-regulated genes (16 PCM genes) and also noticed one group of weakly down-regulated genes in the leaves of the *top6a3* mutant relative to the WT (Supplementary Table S7). Among the 16 PCM genes, three Chl biosynthetic genes (*HEMA*, *HEMB* and *PORA*) were highly up-regulated.

We next compared the transcript levels of Chl biosynthetic genes between K3 and both *top6* mutants by RT–qPCR. Accordingly, we examined 19 functional genes encoding various enzymes acting at one of 15 steps of Chl biosynthesis, which revealed that *HEMA*, *HEMB* and *PORA* are also strongly up-regulated in the mutants (Supplementary Figure S2B). However, these genes were not differentially expressed in the *TOPA3-OE1 TOP6B-OE1* double overexpressing line relative to the WT (Supplementary Figure S1L). These observations support our hypothesis that the higher expression of select Chl biosynthetic genes (*HEMA*, *HEMB* and *PORA*) in the mutants is responsible for the greater accumulation of Chl in these seedlings.

Notably, a previous study reported that Arabidopsis TOP6A directly binds to proximal promoter regions of $^1O_2$-responsive genes and regulates their expression (30). We therefore conducted a ChIP assay to test whether the TOP6 complex might directly regulate the expression of PCM genes by binding to their promoters. As shown in Figure 2D and Supplementary Figure S2A, TOP6A3 indeed bound to the proximal promoter regions of the 13 PCM genes from the up-regulated group (*Lhca2*, *Lhcb1.1*, *Lhcb1a*, *Lhcb2.1*, *Lhcb6*, *PORA*, *HEMB*, *HEMA*, *PsaN*, *PsaO*, *PsbR1*, *PsbQ* and *RbcS1*) in K3 plants following exposure to 4°C. Moreover, the TOP6A3 signal at these promoters was much higher in *TOPA3-OE1* plants grown at the control temperature of 28°C compared with K3 plants.

We selected the two most strongly down-regulated genes (*PsbS* and *FD2*) and three unaffected genes (*Lhcb4*, *PS1-F* and *PsbX*) for ChIP-qPCR, which showed an enrichment of TOP6A3 at the *PsbS* and *FD2* promoters, but not at *Lhcb4*, *PS1-F* or *PsbX* (Figure 2D). We conclude that TOP6A3 mediates a specific regulation under cold stress by directly binding to the promoter regions of at least 15 PCM genes (13 up-regulated genes and 2 down-regulated genes). Further RT–qPCR analysis revealed that the transcript levels of the 13 TOP6A3-bound genes in the up-regulated group are sharply lower in WT seedlings exposed to 4°C for 24 h, with a more modest repression in cold-treated *top6* mutants relative to *top6* mutants grown in control conditions (28°C) (Figure 2C).

Taken together, our data indicate that the TOP6 complex might regulate the two groups of PCM genes in a distinct manner in rice leaves under normal growth. Globally, the TOP6 complex appears to negatively affect the PCM pathway. TOP6A3 binds to the promoter regions of these PCR genes under cold stress, leading us to hypothesize that the TOP6A3 signal is a prerequisite for the cold-induced inhibition of these 13 PCM genes in rice leaves.

A TOP6A3-specific signal occurs at DSB damage sites in the *TOP6A3-OE1 TOP6B-OE1* double overexpressing line

Protein-linked DNA breaks (PDBs) can arise along chromosomes from the inappropriate action of DNA and RNA topoisomerases, which is probably a frequent hazardous event in all forms of life (46,47). To assess whether the rice TOP6 complex binds to DSB sites in somatic cells, we first determined the subcellular localization of TOP6A3 and TOP6B in rice protoplasts. To this end, we fused TOP6A3 and TOP6B individually with GFP and performed a transient expression assay with the encoding constructs. We used a fusion between the TF basic leucine zipper 52 (OsbZIP52) and the RFP as a nuclear marker (40). Upon co-transfection of protoplasts, we visualized the co-localization of GFP and RFP signals in the nucleus, indicating that TOP6A3–GFP and TOP6B–GFP are located in the nucleus (Figure 3A). In our previous report, we used the pSDSA.CON vector to detect homologous recombination (HR)-mediated repair efficiency after DSB induction by the endonuclease I-SceI (48). In this study, we created a new vector (pI-SceI.CON) by removing the I-SceI nuclease gene but keeping its cognate restriction site in the T-DNA region. We then introduced the T-DNA of the pI-SceI.CON vector into K3 callus via *Agrobacterium*-mediated transformation (49). We selected transformed calli based on growth on medium containing hygromycin for 20 days, after which we prepared protoplasts from T_0 generation transgenic calli. Finally, we co-transfected these protoplasts with constructs expressing *TOP6A3* and I-SceI. As shown in Figure 3B, we detected a clear TOP6A3 immunofluorescence signal in the nucleus of protoplasts co-transfected with *TOP6A3* and I-SceI, while we detected no signal when protoplasts were transfected only with I-SceI.

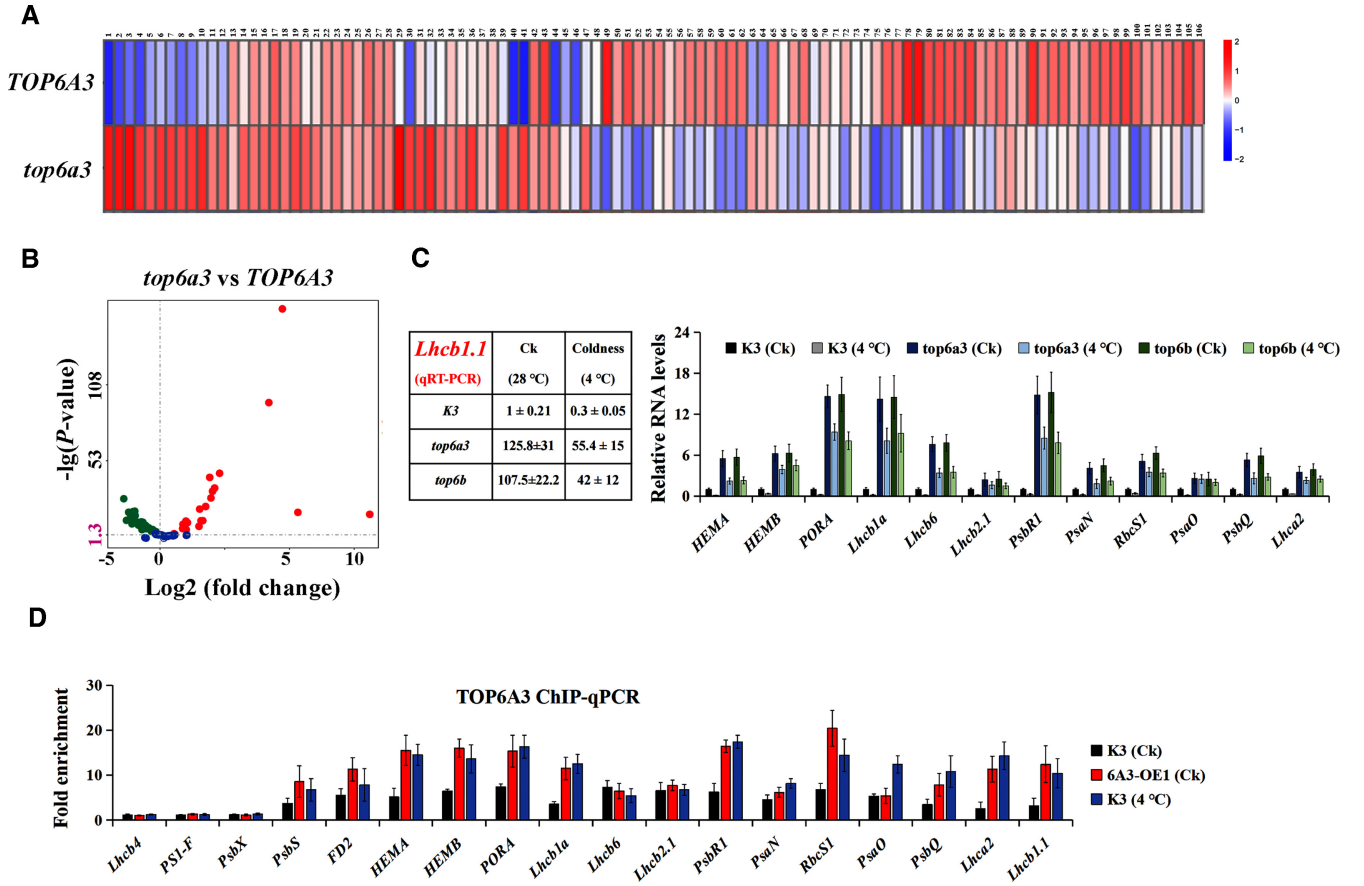

Figure 2. Expression profiles of PCM genes in *top6a3* and WT plants. (**A**) Heatmap representation of the expression levels of global PCM pathway genes in the *top6a3* mutant and WT (K3) seedlings under normal growth conditions ($n = 3$). Rice leaves of the indicated genotypes were collected from 14-day-old seedlings grown on half-strength Murashige and Skoog (MS) medium. The full IDs of the genes shown in the heatmap are listed in Supplementary Table S6. The heatmap is based on FPKM (fragments per kilobase of exon per million mapped fragments) values: blue, low expression; red, high expression. (**B**) Volcano plot of differentially expressed PCM genes between the *top6a3* mutant and WT (K3) plants ($n = 3$). –log10 (*P*-value) >1.3 indicates that differences in gene expression are significant. (**C**) RT–qPCR analysis of 13 PCM genes in rice leaves of the mutants (*top6a3* and *top6b*) and WT (K3) under control conditions (28°C) and cold stress (4°C). Total RNA samples were extracted from the leaves of 2-week-old seedlings. Rice *UBQ* was used for normalization. Experiments were performed three times. Data are means ± SE ($n = 6$). (**D**) TOP6A3 binds to the promoters of 13 up-regulated PCM genes: *HEMA* (Os10g0502400), *HEMB* (Os06g0704600), *PORA* (Os04g0678700), *Lhcb1a* (Os01g0600900), *Lhcb6* (Os04g0457000), *Lhcb2.1* (Os03g0592500), *PsbR1* (Os07g0147500), *PsaN* (Os12g0189400), *RbcS1* (Os02g0152400), *PsaO* (Os04g0414700), *PsbQ* (Os07g0544800), *Lhca2* (Os07g0577600) and *Lhcb1.1* (Os01g0720500). ChIP assays were carried out using anti-TOP6A3 antibodies on the overexpressing line *TOP6A3-OE1* and cold-treated WT (K3) plants (4°C) for 24 h. Anti-histone H3 antibody was used as a non-specific control. Experiments were performed three independent times and the qPCR assay was conducted in triplicate with primers designed to amplify proximal promoter regions. *6A3-OE1*, overexpressing line *TOP6A3-OE1*.

To test whether the rice TOP6 complex can be loaded onto γ-irradiation-induced DSBs, we performed immunostaining assays to detect the TOP6A3 signal in the nuclei of root tip cells following ionization irradiation (IR) at 40 Gy. We did not detect TOP6A3 foci in the nuclei of WT seedlings after IR treatment, whereas we observed strong signals in irradiated *TOP6A3-OE1 TOP6B-OE1* seedlings, with an average number of 45.5 (±8.5) foci per nucleus (nuclei with >5 foci) and 80.1% (±18.1) of nuclei showing >5 foci (Figure 3C; Supplementary Data S6a).

In parallel, to explore whether and how the TOP6 complex affects the cellular response to somatic DSB damage, we analyzed how seedlings from each overexpressing line responded to genotoxic stress. Accordingly, we measured the height of seedlings from each overexpressing line and the WT K3 after 14 days of growth on half-strength Murashige and Skoog (MS) medium alone or containing different concentrations of the genotoxic drugs bleomycin (BLM) or mitomycin C (MMC). As shown in Figure 3D, Supplementary Figure S3E and Supplementary Data S3, seedlings from the overexpressing lines were shorter than WT seedlings when grown in the presence of 10 μg ml^{-1} BLM or 20 μg ml^{-1} MMC. However, *TOP6A3-OE1* and *TOP6B-OE1* seedlings had a normal height when grown in the presence of a lower concentration of BLM (2 μg ml^{-1}), unlike c-NHEJ mutants (*ku70* and *lig4*), whose growth was clearly repressed by this low BLM dose (Figure 3F and G; Supplementary Data S4). This result is in line with the fact that *ku70* and *lig4* mutants are more vulnerable to BLM than the *TOP6A3-OE1* and *TOP6B-OE1* seedlings. In an independent approach, we γ-irradiated seeds, which we then germinated to assess the growth parameters of the resulting seedlings. Following

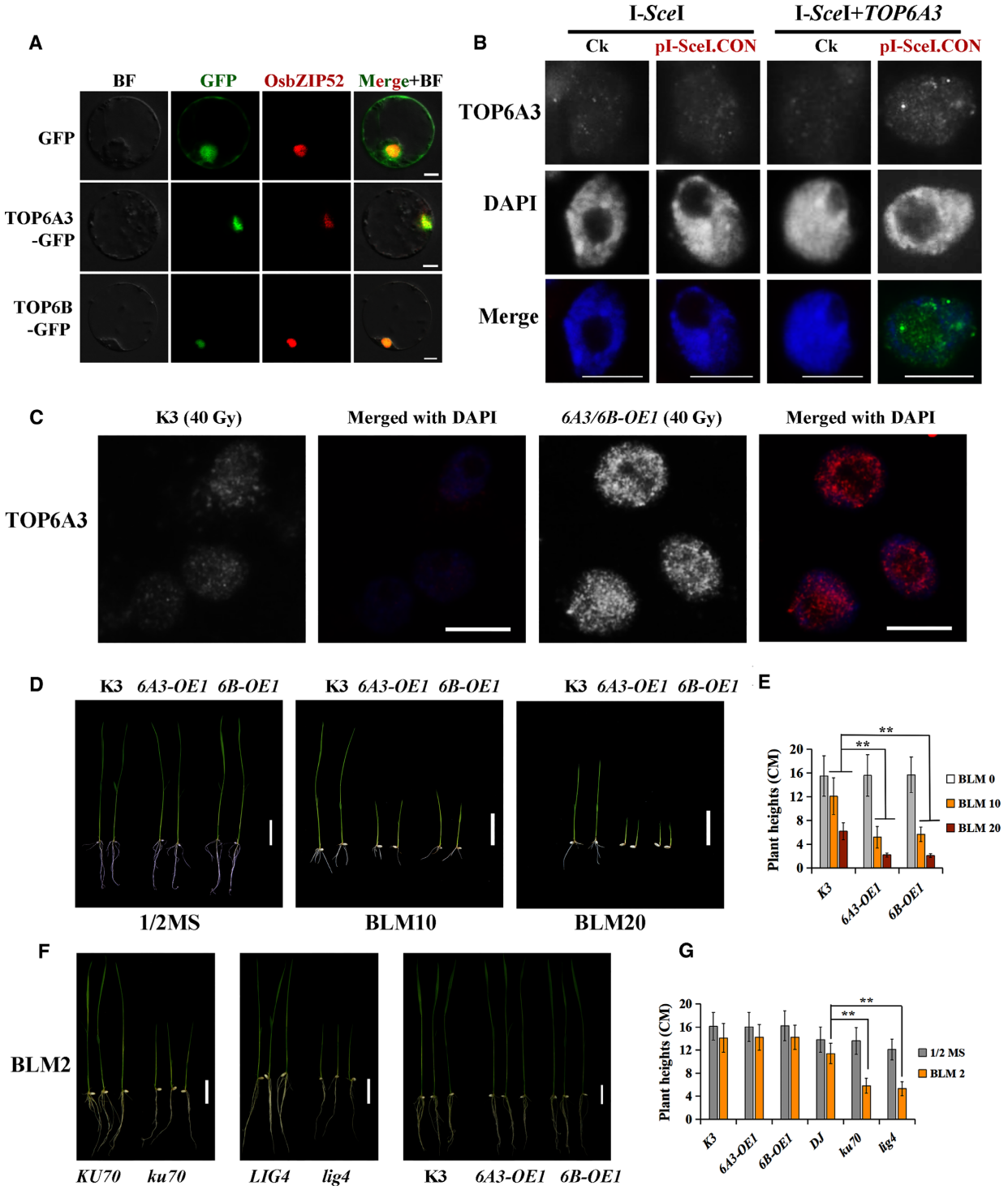

Figure 3. Subcellular localization of TOP6A3 and TOP6B, immunostaining of TOP6A3 in callus protoplast and root tips, and genotoxic sensitivity assays of *TOP6A3-OE1* and *TOP6B-OE1* plants. (**A**) Subcellular localization of TOP6A3 and TOP6B in rice protoplasts. OsbZIP52–RFP was used as a nuclear marker. BF, brightfield. Scale bars, 10 μm. (**B**) Immunofluorescence staining of TOP6A3 in protoplast nuclei with or without I-SceI restriction sites, after co-transfection of *TOP6A3* and I-SceI. pI-SceI.CON designates a vector containing the restriction site for the endonuclease I-SceI in the T-DNA region. I-SceI, I-SceI nuclease. Scale bars, 10 μm. (**C**) Immunofluorescence staining of TOP6A3 in nuclei isolated from rice root tips of *TOP6A3-OE1* *TOP6B-OE1* and WT (K3) seedlings after irradiation. Samples were collected 20 min after an exposure to 40 Gy irradiation. Blue, DAPI-stained nuclei; red, immunofluorescence signals. Scale bars, 10 μm. (**D**) Growth retardation of *TOP6A3-OE1* and *TOP6B-OE1* seedlings after 9 days of growth on half-strength Murashige and Skoog (1/2 MS) medium containing 10 or 20 μg ml^{-1} bleomycin (BLM). Scale bars, 3 cm. (**E**) Mean height for the *TOP6A3-OE1*, *TOP6B-OE1* and WT (K3) seedlings depicted in (D). (**F**) The c-NHEJ pathway mutants *ku70* and *lig4* are more vulnerable to BLM treatment than the overexpressing lines *TOP6A3-OE1* and *TOP6B-OE1* after 9 days of growth on 1/2 MS medium containing 2 μg ml^{-1} BLM. Scale bars, 2 cm. (**G**) Mean height of mutants (*ku70* and *lig4*) and overexpressing lines *TOP6A3-OE1* and *TOP6B-OE1* shown in (F). *6A3-OE1*, *6A3-OE1* overexpressing line; *6B-OE1*, *6B-OE1* overexpressing line; *6A3/6B-OE1* double overexpressing line.

γ-irradiation with 100 Gy, the seedlings from both single overexpressing lines showed lower Chl contents in their leaves compared with the WT (Supplementary Figure S3A, B), with a drop of 76% and 74% in *TOPA3-OE1* and *TOP6B-OE1* seedlings, respectively, relative to the WT (Supplementary Data S5). Together, these results clearly indicate that overexpressing *TOP6* genes in rice enhances sensitivity to somatic DSB damage at the post-germination stage.

The phosphorylation of histone H2AX (γ-H2AX) is one of the earliest events to occur in response to DSBs and is used as a highly specific biomarker for monitoring DSBs (50,51). To cytologically probe the efficiency of DSB repair, we thus performed γ-H2AX immunostaining in the nuclei of root tip cells in the overexpressing lines (*TOPA3-OE1* and *TOP6B-OE1*) and mutants (*top6a3* and *top6b*) grown on half-strength MS medium alone or containing 20 μg ml^{-1} BLM (Supplementary Figure S3C, D). Notably, we detected higher γ-H2AX signals (average number of nuclei with >5 foci) in BLM-treated overexpressing lines (2.17 and 2.19 times higher in *TOPA3-OE1* and *TOP6B-OE1*, respectively), relative to BLM-treated WT seedlings (Supplementary Figure S3D; Supplementary Data S6b). In contrast, the γ-H2AX signals were comparable between BLM-treated mutants (*top6a3* and *top6b*) and the WT (Supplementary Figure S3C, D).

Overall, the TOP6A3-specific signals observed at somatic DSB sites and the hypersensitive phenotypes of *TOP6A3-OE1* and *TOP6B-OE1* seedlings to genotoxic drugs indicate that the TOP6 complex negatively regulates the efficiency of DSB repair by repressing the targeted DSB repair pathway in rice somatic cells.

TOP6A3 specifically decreases the binding capacity of KU70 to DSB sites, which is facilitated by its partner TOP6B

A Y2H assay previously showed that AtSPO11-3 interacts with AtTOP6B [also named ELONGATED HYPOCOTYL 6 (HYP6)] (44). We therefore asked whether rice TOP6A3 and TOP6B might interact as well. To this end, we cloned the coding sequences of *TOP6A3* and *TOP6B* individually into yeast vectors harboring the GAL4 activation domain (AD) or GAL4 DNA-binding domain (BD). Positive yeast transformants carrying both constructs grew on quadruple dropout medium (Supplementary Figure S4), indicating that indeed TOP6A3 and TOP6B interact; we also observed that each TOP6 protein can homodimerize.

Meiotic HR is initiated by the formation of a DSB site that is generated by SPO11 (24). As the c-NHEJ pathway acts predominantly during somatic DSB repair in most higher eukaryotes, we asked whether the rice TOP6 complex might interact with the proteins (KU70 and KU80) of the first step of the c-NHEJ pathway. Accordingly, we tested the interaction between full-length TOP6A3 or TOP6B and KU70 or KU80 in a Y2H assay, which revealed an interaction between TOP6A3 and KU70 (Figure 4A). However, we observed no interaction between TOP6B and KU70, TOP6A3 and KU80, or TOP6B and KU80. We also tested these interactions in pull-down assays by mixing recombinant purified GST and histidine (HIS) fusion proteins (GST–TOP6A3, GST–TOP6B and KU70-HIS). We successfully detected KU70-HIS following GST pull-down of GST–TOP6A3, but not of GST–TOP6B (Figure 4B), confirming that TOP6A3 and KU70 interact *in vitro*. We expanded our assays *in vivo* by performing a firefly luciferase (LUC) complementation imaging assay. We transiently infiltrated constructs encoding TOP6 (TOP6A3 or TOP6B) fused with the C-terminus of LUC (cLUC-TOP6A3 and cLUC-TOP6B) and the N-terminus of LUC fused with KU70 (KU70-nLUC) into *N. benthamiana* leaves. We detected luminescence signals in leaf regions co-expressing *KU70-nLUC* and *cLUC-TOP6A3*, but not *KU70-nLUC* and *cLUC-TOP6B* (Figure 4D). We conclude that KU70 and TOP6A3 interact *in vitro* and *in vivo*.

Because the KU complex binds to DSB sites to initiate the KU-mediated c-NHEJ pathway, we next examined whether the TOP6A3×KU70 interaction might affect the association of KU70 with DSBs in an EMSA. We determined that recombinant KU70 can bind to a small nonspecific DNA fragment (150 bp in length), used here to simulate a DSB terminal *in vitro* (Figure 4C). With the addition of recombinant TOP6A3 to the reaction, we observed a decrease in the intensity of the shifted signal (Figure 4C), suggesting that TOP6A3 may represses the binding of KU70 to DSBs via direct protein–protein interaction. As an important control, neither recombinant TOP6A3 nor TOP6B showed any binding to the DNA probe (Figure 4C). Moreover, adding both recombinant TOP6A3 and TOP6B to the reaction further diminished the strength of KU70–DNA binding (Figure 4C). This result indicates that TOP6B facilitates the TOP6A3-mediated inhibition of KU70 loading at DSB terminals *in vitro*.

We examined whether overexpression of *TOP6* genes has an effect on loading of the key factors in the DSB pathway to DSB sites. Here, we conducted immunofluorescence assays on the nuclei of root tip cells from the WT and the double overexpressing line *TOPA3-OE1 TOP6B-OE1* following IR treatment to measure the strength of immune signals specific to the c-NHEJ factor LIG4, the alt-NHEJ factor COM1 and the HR factors RAD51C and RAD51 (Figure 4E, F). Compared with the WT, we counted comparable numbers of foci for RAD51, RAD51C and COM1 in *TOP6A3-OE1 TOP6B-OE1*, whereas the number of LIG4 foci decreased 11.9 ± 3.9% (Supplementary Data S6e).

Together, these biochemical tests indicate the TOP6A3 specifically interacts with the c-NHEJ factor KU70 to decrease its capacity to bind to DSB sites, which is facilitated by its partner TOP6B to cooperatively repress the KU-mediated c-NHEJ pathway.

TOP6 genes are required for the induced expression of the HR gene *RAD51A2* following bleomycin treatment, while mutations have no effect on irradiation-induced γ-H2AX kinetics

Our findings that both *TOP6A3-OE1* and *TOP6B-OE1* exhibit hypersensitive phenotypes to genotoxic drugs (Figure 3D; Supplementary Figure S3A) prompted us to examine whether the *TOP6* genes might modulate the expression of key genes in DSB repair pathways. We therefore analyzed the transcript levels of these genes in 1-week-old seedlings of *top6a3* and *top6b* single mutants grown under control con-

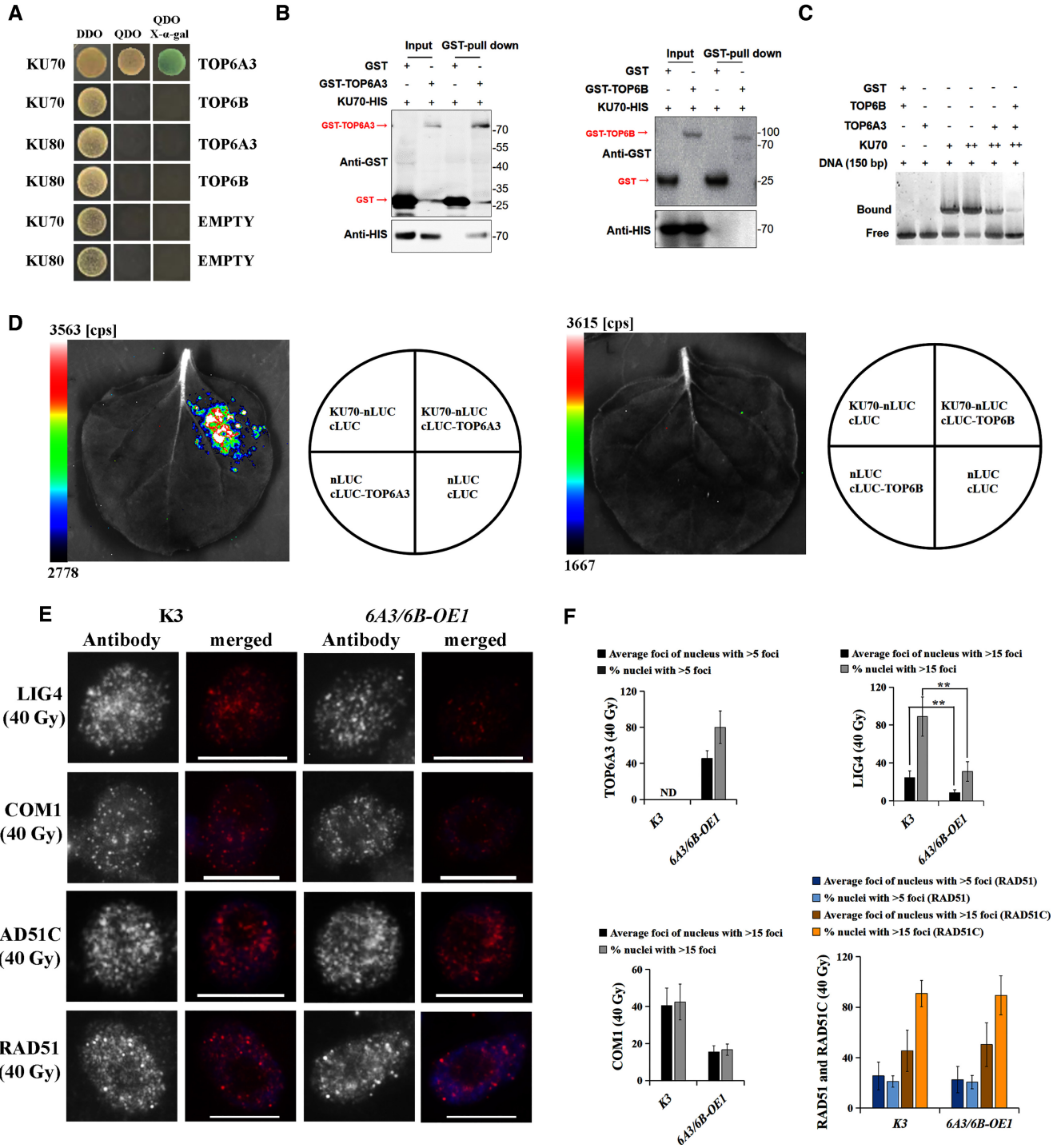

Figure 4. TOP6A3 physically interacts with KU70 and inhibits its binding to a non-specific DNA fragment, immunostaining signals of key DSB repair factors in the double overexpressing line *TOP6A3-OE1 TOP6B-OE1* and WT seedlings following irradiation. (**A**) TOP6A3 interacts with KU70 in a Y2H assay. DDO, double dropout medium. QDO, quadruple dropout medium. (**B**) Pull-down assay showing that TOP6A3, not TOP6B, interacts with KU70. GST fusion proteins were immobilized onto Glutathione Sepharose 4B resin, to which HIS fusion proteins were added. The pulled down proteins were separated by 10% SDS–PAGE and immunoblotted with anti-HIS or anti-GST antibody. Arrows indicate the GST-tagged proteins. (**C**) EMSA showing that TOP6A3 and TOP6B affect the binding of KU70 to a non-specific DNA fragment. (**D**) Luciferase complementation imaging assay showing that TOP6A3 and KU70 interact with each other in *N. benthamiana* leaves. *Agrobacterium* colonies harboring different constructs were infiltrated into *N. benthamiana* leaves. Two days after infiltration, luciferase activity was recorded with a CCD camera. cps, counts per second. (**E**) Immunofluorescence staining of NHEJ factors (LIG4 and COM1) and HR factors (RAD51C and RAD51) in nuclei isolated from rice root tips of the double overexpressing line *TOP6A3-OE1 TOP6B-OE1* and WT (K3) seedlings post-IR. Samples were collected 20 min after being exposed to 40 Gy. Blue, DAPI-stained nuclei; red, signal from the indicated antibodies. Scale bars, 10 μm. (**F**) Quantification of the immunostaining signals shown in (E). ($P < 0.01$, by Student's *t*-test). Data are means ± SD ($n = 3$). **Significant difference between K3 and the overexpressing line, *P*-value <0.01, as determined by a Student's *t*-test. ND, no signal detected. *6A3/6B-OE1*, double overexpressing line.

ditions and in the presence of 10 μg ml^{-1} BLM for 24 h by RT–qPCR. Compared with the WT, the HR pathway gene *RAD51A2* failed to be normally induced by the BLM treatment, whereas all other c-NHEJ genes tested (*KU70*, *KU80* and *LIG4*) showed a slight increase in transcript levels in both single mutants (Supplementary Figure S5A). Furthermore, ChIP-qPCR analysis indicated that TOP6A3 binds to the proximal promoter region of *RAD51A2* after γ-irradiation treatment of 40 Gy, but not to the promoters of other c-NHEJ genes (*KU70*, *KU80* and *LIG4*) (Supplementary Figure S5B). This result indicates that TOP6A3 directly binds to the *RAD51A2* promoter, which may be crucial for its induction during the DSB damage response.

To uncover whether the loss of *TOP6* function affects the efficiency of DSB repair in rice somatic cells, we investigated the γ-H2AX signals in the nuclei of root tip cells from irradiated WT and mutant (*top6a3* and *top6b*) seedlings after 6, 12 or 24 h of IR treatment. Unlike the *TOP6A3-OE1* and *TOP6B-OE1* single overexpressing lines, we observed normal γ-H2AX kinetics in both single mutants post-IR treatment, relative to irradiated WT seedlings (Supplementary Figure S5C, D).

Together, these results indicate that the TOP6 complex is indispensable for the transcriptional induction of *RAD51A2* during the DSB response, while the loss of *TOP6* function did not affect DSB repair efficiency, based on the kinetics of γ-H2AX accumulation.

The TOP6 complex attenuates c-NHEJ repair efficiency in MCs under cold stress

Cold stress causes DNA fragmentation and programmed cell death (PCD) in tobacco (*Nicotiana tabacum*) BY-2 cells (52), maize (*Zea mays*) and Arabidopsis in the nuclei of root tip cells (53,54). We thus wished to investigate the occurrence of DNA fragmentation in rice MCs subjected to cold stress. Accordingly, we performed a comet assay and γ-H2AX immunostaining on the nuclei of MCs from the WT K3 after a 24 h cold treatment (Figure 5A, B). Notably, we observed clear comet tails in cold-treated leaves, but not in control samples (Figure 5A, E). In agreement, we also detected γ-H2AX-positive foci in nuclei, with an average of 15 (± 5.2) foci per nucleus (with >5 foci), with 41 (± 16.3)% of the nuclei showing >5 foci (Figure 5B, F). These results indicate that rice MCs are prone to DNA damage in response to cold stress.

Immunoblot analysis indicated that TOP6A3 abundance rises in the WT after cold treatment (Figure 5D). We thus asked whether the TOP6 complex represses DSB repair efficiency in cold-treated MCs. To answer this question, we performed γ-H2AX immunostaining and comet assays in the nuclei of MCs from the mutants (*ku70*, *top6a3* and *top6b*) and the double overexpressing line (*TOP6A3-OE1 TOP6B-OE1*) grown at 28°C (control conditions) and following cold treatment. We detected lower γ-H2AX signals (average foci of nucleus with >5 foci) in both cold-treated mutants (Figure 5B), with an average of 8.7 (± 3.5) and 3.5 (± 4.5) foci in *top6a3* and *top6b*, respectively, compared with 15 in the WT (Figure 5F; Supplementary Data S6f). However, the γ-H2AX signal increased in *TOP6A3-OE1 TOP6B-OE1* seedlings relative to the WT (Figure 5B, F). The comet tail moment was consistent with the γ-H2AX signals, which a smaller moment in both mutants and a greater moment in *TOP6A3-OE1 TOP6B-OE1* seedlings (Figure 5A, E). Importantly, the c-NHEJ pathway mutant (*ku70*) produced more DSB damage signals than the *TOP6A3-OE1 TOP6B-OE1* double overexpressing line in cold-treated MCs (Figure 5E, F). Together, these results show that the TOP6 complex attenuates DSB repair efficiency in cold-treated MCs and that the *ku70* mutant displays more severe defects than the *TOP6A3-OE1 TOP6B-OE1* double overexpressing line under cold stress.

We examined whether cold stress might trigger the loading of the TOP6 complex at DSB sites in the nuclei of MCs. As shown in Figure 6A, we detected few TOP6A3 foci in nuclei of seedlings grown at normal temperature (28°C), whereas we observed bright TOP6A3-positive foci following cold treatment (4°C), with an average of 15.5 (±4.5) foci per nucleus (with >5 foci), and 82.1% (±12.8) of nuclei with >5 foci (Figure 6D; Supplementary Data S6a).

As we had observed that overexpression of *TOP6* genes causes a decrease in LIG4 loading at DSB sites in irradiated root tips (Figure 4E, F), we wished to ask whether the TOP6 complex induced by cold treatment might repress the DSB repair factors at cold-induced DSB sites. We thus examined the immune signals for each of these factors in MCs after cold treatment. As shown in Figure 6B, we observed a comparable signal strength and number of foci for COM1 in all seedlings regardless of treatment, whereas the LIG4 signal in cold-treated WT seedlings only reached ∼11.3 (±2.3)% of that seen in the *top6a3* mutant under cold stress (Supplementary Data S6c). Moreover, we only detected immune signals for HR factors (RAD51 and RAD51C) in the nuclei of MCs following a combined cold and γ-irradiation treatment, but not in nuclei only exposed to cold stress (Figure 6C, D). However, we detected no obvious difference between the *top6a3* mutant and K3 for these two factors in response to combined cold and γ-irradiation treatment (Supplementary Data S6d).

Overall, these results support the notion that accumulation of the TOP6 complex at cold-induced DSB sites prevents LIG4 loading, which contributes to the attenuation of c-NHEJ repair efficiency in rice MCs under cold stress.

The ATM kinase is pivotal for the DSB damage response-mediated transcriptional suppression of PCM genes

We established here that K3 seedlings germinated from γ-irradiated seeds have light green leaves with a decrease in total Chl contents compared with control seedlings germinated from non-irradiated seeds (Supplementary Figure S3A, B). We wondered whether DSB damage might result in a short-term repression of photosynthesis-related gene expression in rice leaves. To test this idea, we firstly conducted an RNA-seq analysis of rice leaves from the rice cultivar Dongjin (DJ) without or with γ-irradiation treatment of 40 Gy. We identified 775 DEGs between the control condition and γ-irradiation treatment (Supplementary Table S7). A Kyoto Encyclopedia of Genes and Genomes (KEGG) pathway enrichment analysis showed that DEGs in irradiated seedlings are mainly related to photosynthesis, photosynthesis-antenna proteins, carbon metabolism and

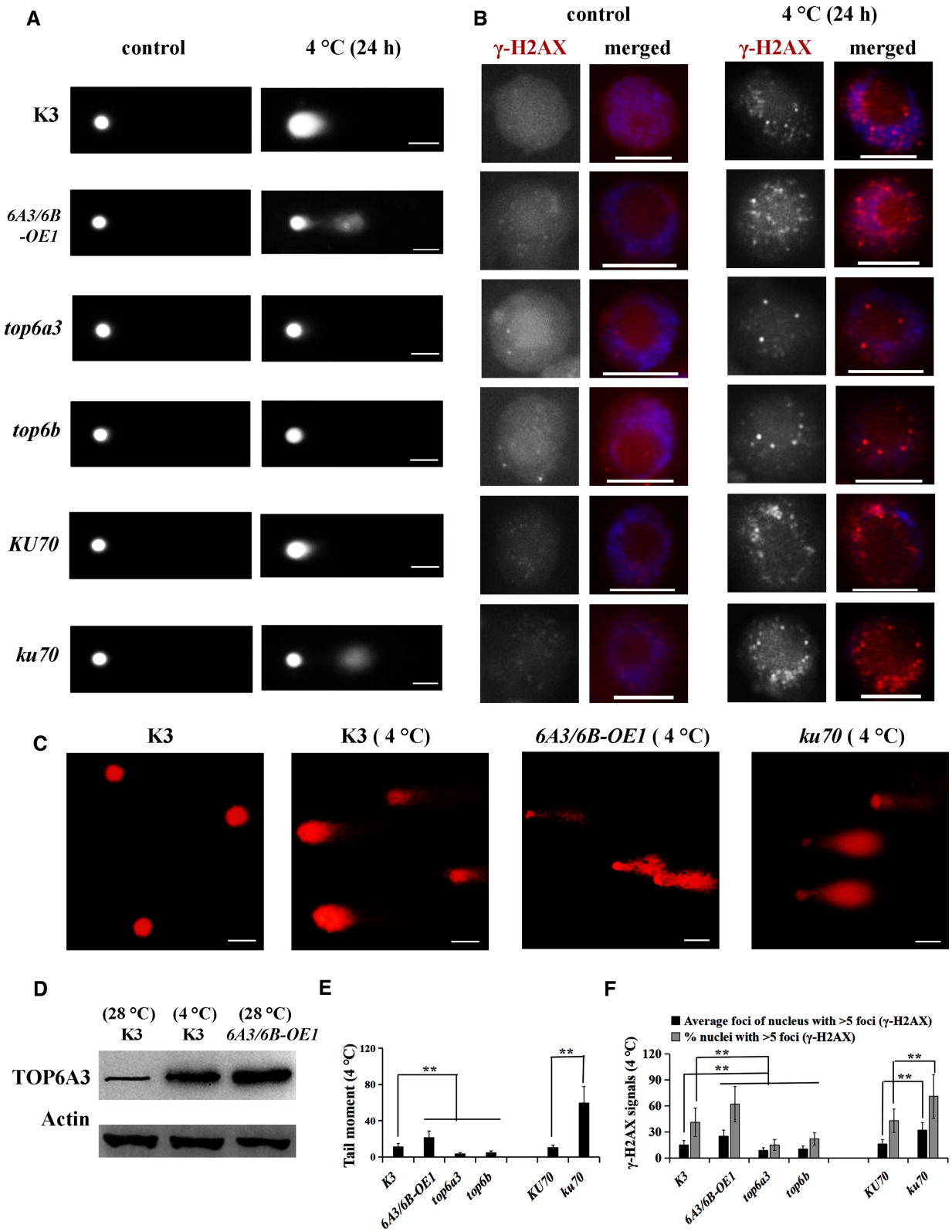

Figure 5. γ-H2AX immunostaining and comet assays in the double overexpressing line *TOP6A3-OE1 TOP6B-OE1*, mutants (*top6a3*, *top6b* and *ku70*) and the WT 24 h after cold exposure. (**A**) Comet assays showing the nucleus of single MCs from mutants (*top6a3*, *top6b* and *ku70*), the double overexpressing line (*6A3/6B-OE1*) and K3 seedlings after 24 h of cold treatment at 4°C. Scale bars, 20 μm. (**B**) γ-H2AX immunostaining assays of the nucleus of single MCs. Scale bars, 10 μm. (**C**) Comet assays with multiple MC nuclei from the *ku70* mutant, the double overexpressing line *6A3/6B-OE1* and K3 seedlings after 24 h of cold treatment at 4°C. Scale bars, 20 μm. (**D**) Immunoblot analysis of TOP6A3 abundance in control rice leaves of the WT (K3), the double overexpressing line (*6A3/6B-OE1*) and cold-treated K3 seedlings at 4°C for 24 h. ACTIN served as a loading control. (**E**) Quantification of the comet tail moment in (A). (**F**) Quantification of the γ-H2AX signals in (B) For (E) and (F), data are means ± SD ($n = 3$). **significant difference compared with the WT, *P*-value <0.05 as calculated by on one-way ANOVA. *6A3/6B-OE1*, double overexpressing line.

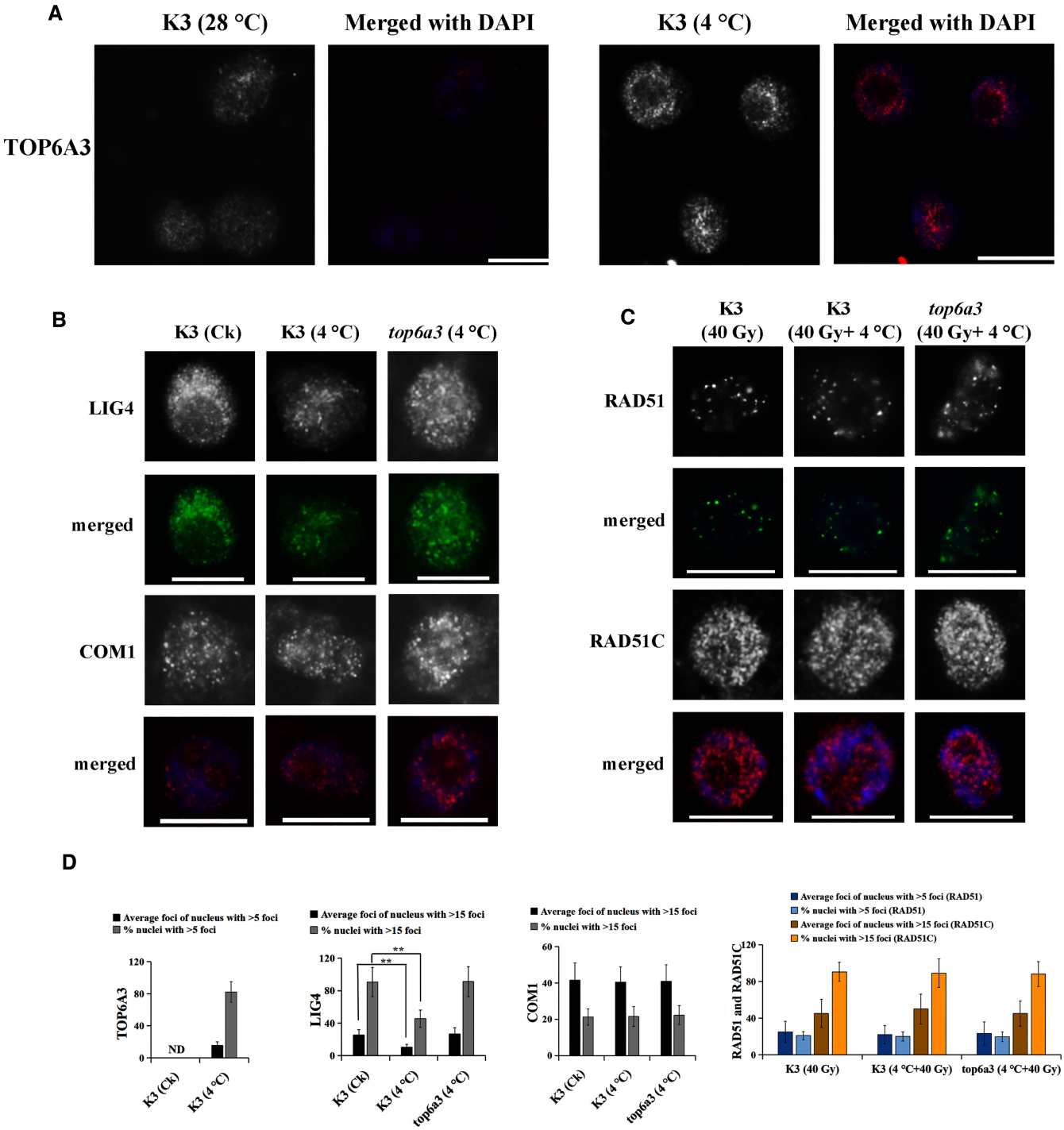

Figure 6. Immunostaining assays of TOP6A3 in cold-treated WT (K3), NHEJ factors (COM1 and LIG4) in cold-treated K3 and *top6a3* mutant seedlings, and HR factors (RAD51 and RAD51C) in K3 and *top6a3* mutant seedlings subjected to combined cold and irradiation treatments. (**A**) Immunofluorescence staining of TOP6A3 in nuclei isolated from rice MCs of K3 seedlings under both control and cold treatment. Leaf samples were collected after 24 h of cold treatment at 4°C. Blue, DAPI-stained nuclei; red, signal from antibodies. Scale bars, 10 μm. (**B**) Immunofluorescence staining of NHEJ factors (LIG4 and COM1) in nuclei isolated from rice MCs from the *top6a3* mutant or WT (K3) seedlings following cold treatment. Leaf samples were collected after 24 h of cold treatment at 4°C. Blue, DAPI-stained nuclei; red, signal from antibodies. Scale bars, 10 μm. (**C**) Immunofluorescence staining of HR factors (RAD51C and RAD51) in nuclei isolated from rice MCs from the *top6a3* mutant or WT (K3) seedlings exposed to both cold (4°C) and γ-irradiation (40 Gy). The cold-treated leaf samples were collected 20 min after exposure to 40 Gy irradiation. Blue, DAPI-stained nuclei; red, signal from antibodies. Scale bars, 10 μm. (**D**) Quantification of the immunostaining signals in (A–C). Data are means ± SD ($n = 3$). ND, not detected. **Significant difference compared with K3 seedlings under control conditions, $P < 0.01$, as calculated using a Student's *t*-test.

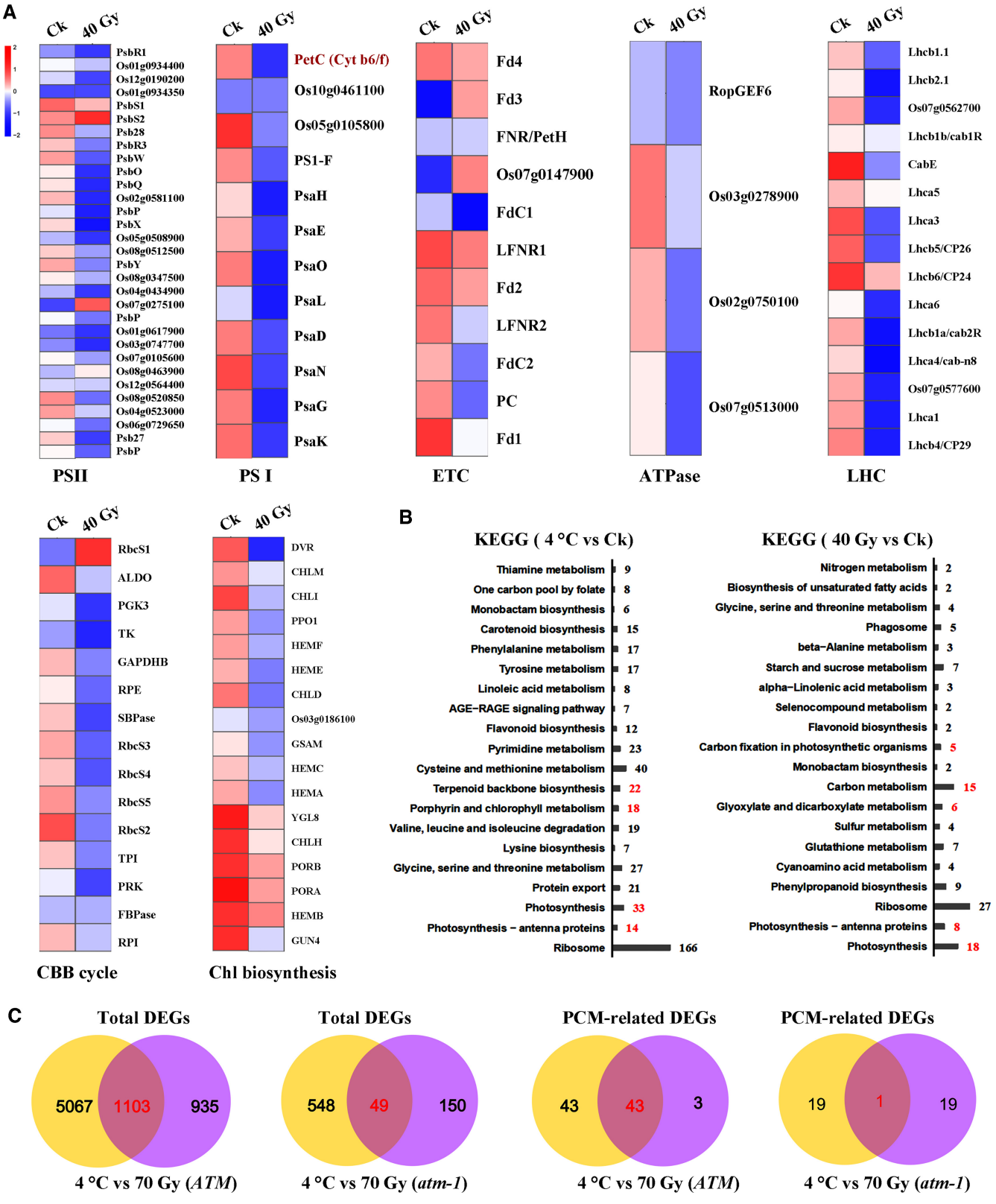

Figure 7. Analysis of global PCM gene expression from RNA-seq data after γ-irradiation, and KEGG analysis and Venn diagrams in rice leaves after γ-irradiation or cold treatments. (**A**) Heatmap representation of expression levels from down-regulated PCM genes in response to γ-irradiation (40 Gy; $n = 3$). Rice leaves of Dongjin (DJ) were collected after 6 h exposure to irradiation of 40 Gy. CBB cycle, Calvin–Benson–Bassham cycle; ETC, electron transport chain; LHC, light-harvesting chlorophyll protein complex. The heatmap is based on FPKM values of all samples. Blue, low expression; red, high expression. (**B**) KEGG pathway analysis of DEGs in rice leaves exposed to γ-irradiation or cold conditions. (**C**) Venn diagrams showing the extent of overlaps between DEGs for γ-irradiation or cold treatment in the *atm-1* mutant and WT.

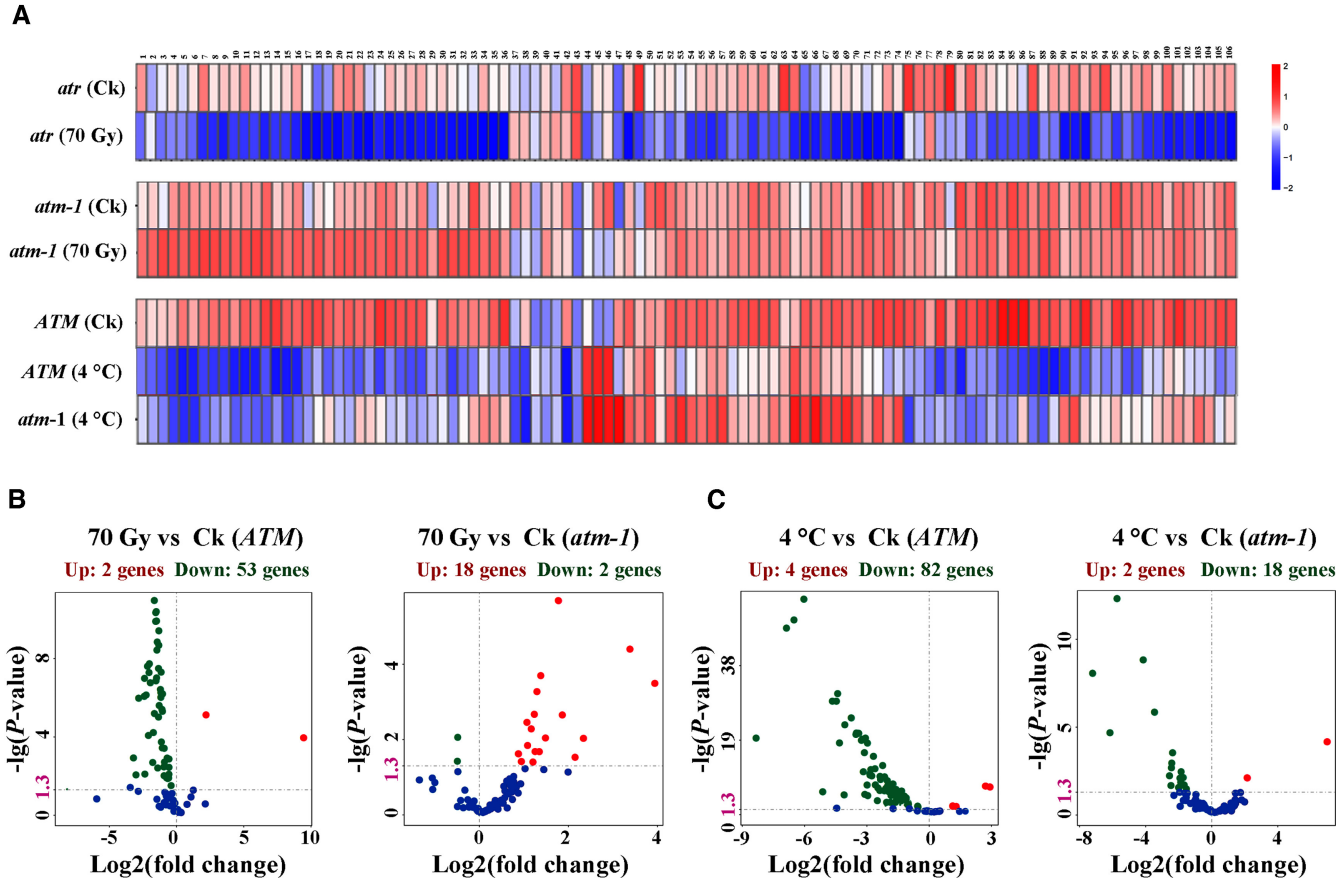

Figure 8. Heatmap representation of the global expression of PCM genes in irradiated *atm-1*, *atr*, WT (K3) and cold-treated WT and *atm-1* seedlings. (**A**) Heatmap representation of the expression levels of 106 PCM genes in irradiated mutant seedlings (*atm-1* and *atr*) and cold-treated seedlings (WT and *atm-1*) ($n = 3$). Rice leaves were collected 6 h after exposure to 70 Gy irradiation, or after 24 h of cold treatment (4°C). The full IDs of the PCM genes used in the heatmap are given in Supplementary Table S6. (**B**) Volcano plots of PCM-related DEGs in the *atm-1* mutant and its WT (*ATM*) after treatment by γ-irradiation ($n = 3$). Rice leaves were collected after 6 h exposure to IR (40 Gy). –log10 (*P*-value) >1.3 indicates that differences in gene expression are significant. Green, down-regulated DEGs; red, up-regulated DEGs. (**C**) Volcano plots of PCM-related DEGs in the *atm-1* mutant and its WT (*ATM*) after cold treatment ($n = 3$). Rice leaves were collected after cold treatment for 24 h at 4°C. –log10 (*P*-value) >1.3 indicates that differences in gene expression are significant. Green, down-regulated DEGs; red, up-regulated DEGs.

phenylpropanoid biosynthesis (Figure 7B). A comparison of the KEGG analysis results between seedlings treated with γ-irradiation or cold revealed that photosynthesis-related pathways are the most overlapping in rice leaves (Figure 7B). Moreover, Venn diagram assays between the γ-irradiation and cold treatments indicated that 1103 DEGs and 43 PCM-related DEGs are shared in WT (*ATM*) seedlings; however, only 49 DEGs and one PCM-related DEG overlapped between the two treatment in the *atm-1* mutant (Figure 7C).

After γ-irradiation treatment, 53 PCM genes were down-regulated and two PCM genes were up-regulated in leaves (Figures 7A and 8B). Among the down-regulated genes (SupplementaryTable S7), we noticed genes encoding Chl *a*/*b*-binding proteins (Cab E, Lhca4, Lhcb1a, b, CP29 and CP24), PSII components (PsbR3, PsbW and PsbY), PSI reaction center subunits (PSI-F, PsaK, PsaN and PsaO), the cytochrome b_6f complex, chloroplast ATP synthase subunits (delta chain, subunit b and gamma) and other electron transport chain components (Fd1, FdC2, LFNR1 and PC). Furthermore, several genes encoding enzymes participating in the CBB cycle, namely fructose bisphosphate aldolase, transketolase, phosphoribulokinase, glyceraldehyde phosphate dehydrogenase and Rubisco, were also down-regulated upon γ-irradiation treatment. Thus, we speculated that the transcription of various PCM genes might be immediately repressed in response to γ-irradiation.

In eukaryotes, the initial stages of the response to somatic DSB damage are governed by protein kinases ATAXIA-TELANGIECTASIA MUTATED (ATM) (55) and ATM AND RAD3-RELATED (ATR) (56). In a recent report (57), the Arabidopsis ATR–SOG1 (SUPPRESSOR OF GAMMA RADIATION 1) signaling module was shown to regulate pleiotropic phenotypes in response to 3′-blocked DNA repair intermediates. Hence, we asked whether ATM and ATR might play a role in triggering transcriptional suppression of photosynthesis-related genes during the DSB damage response. Accordingly, we examined the expression of all PCM genes after a 6 h recovery period following γ-irradiation (70 Gy). As shown in Figure 8A and Supplementary Table S7, relative to normal conditions, we observed the same transcriptional repression of PCM genes in irradi-

ated *atr* mutant seedlings, as in irradiated DJ seedlings. In contrast, irradiated *atm* mutant seedlings maintained high expression levels for most PCM pathway genes (Figure 8A; Supplementary Table S7), with only two down-regulated and 18 up-regulated PCM genes (Figure 8B).

Altogether, this above RNA-seq analysis indicates that photosynthesis constitutes the most enriched process among DEGs of rice seedlings responding to γ-irradiation stress. We also determined that ATM, but not ATR, controls the γ-irradiation-triggered transcriptional suppression of PCM genes in rice.

TOP6A3 overexpression causes hypersensitivity of photosynthetic parameters under cold stress in an ATM-dependent manner

Our results thus far showed that *TOPA3-OE1* and *TOP6B-OE1* overexpression leads to hypersensitivity to genotoxic drugs and an attenuated DSB repair efficiency in the window of γ-H2AX signals (Figure 3D; Supplementary Figure S3C). Moreover, the RNAs-seq data indicated that PCM pathway genes are quickly transcriptionally repressed in response to γ-irradiation (Figure 7A), which prompted us to examine the expression of PCM genes in irradiated *TOPA3-OE1* seedlings. We observed a more severe down-regulation of PCM genes in *TOPA3-OE1* seedlings after 6 h of γ-irradiation treatment (40 Gy) compared with K3 seedlings (Figure 9A).

To unravel the physiological relevance of *TOP6* genes in rice, we assessed the response of some photosynthetic parameters to cold stress in *TOPA3-OE1* and K3 seedlings (Figure 9B; Supplementary Data S7). Under cold stress, the light-saturated photosynthesis (A_{sat}) of *TOP6A3-OE1* seedlings was 15% lower than that in WT seedlings. Similarly, compared with cold-treated WT seedlings, stomatal conductance (g_s) and intrinsic water use efficiency (*i*WUE) were also significantly lower in cold-treated *TOP6A3-OE1* seedlings, while their CO_2 concentration in the intercellular air space (C_i) was significantly higher. Furthermore, cold-treated *TOP6A3-OE1* seedlings also showed a substantial decline in the electron transport rates (ETRs) around PSI and PSII that was concomitant with a considerable reduction in their quantum yields of the photochemical energy conversion (YII) and (YI). Therefore, overexpression of the *TOP6* genes in rice leads to global declines in photosynthetic parameters under cold stress.

Compared with normal growth conditions at 28°C, RNA-seq analysis revealed that 82 PCM genes are down-regulated and only four PCM genes were significantly up-regulated in K3 seedlings under cold treatment. Importantly, in the leaves of cold-treated *atm-1*, we only detected 18 down-regulated and two up-regulated PCM genes (Figure 8C; Supplementary Table S7). As shown by a heatmap, the *atm-1* mutant largely suppressed the cold treatment-imposed suppression of PCM gene expression seen in WT seedlings (Figure 8A). We conclude that besides the DSB damage response, ATM also plays a pivotal role for the inhibition of PCM gene expression during the cold response.

We explored the genetic relationship between *ATM* and *TOP6* genes. We measured photosynthetic parameters in *TOPA3-OE1 atm* seedlings under cold stress and PCM gene expression post-IR treatment. Unlike the *TOPA3-OE1* seedlings, *TOPA3-OE1 atm* seedlings displayed no hypersensitivity concerning photosynthetic parameters under cold stress (Figure 9B) and also showed no transcriptional inhibition of PCM pathway genes following γ-irradiation treatment (Figure 9A).

In summary, cold stress up-regulates TOP6 complex abundance, which extends DSB damage signaling to prolong the inhibition of photosynthesis in rice leaves. The DSB signal transducer *ATM* might act downstream of *TOP6A3* for the cold-conditioned photosynthesis machinery in rice.

DISCUSSION

PCM constitutes a very complex process orchestrated through a serial of reactions catalyzed by numerous enzymes (58–60) and is highly sensitive to environmental stresses (61,62). Low-temperature stress is a major abiotic factor limiting crop growth, productivity and geographical distribution (3,63). In rice, cold stress inhibits both Chl biosynthesis and chloroplast biogenesis (45), resulting in dramatically lower photosynthetic parameters in leaves (64). Our current study revealed that the coordination of cold stress and the photosynthetic pathway in rice is controlled by the cold-induced DSB damage response and that the DSB mediator ATM acts as a major regulator for the short-term repression of PCM gene expression under cold stress. Notably, we showed that the TOP6 complex modulates PCM gene expression by performing two distinct regulatory tasks: that of a transcriptional regulator that is indispensable for cold-repressed expression of 13 PCM genes, and that of an inhibitor of c-NHEJ to reduce DSB repair efficiency and thereby prolong the DSB damage response-mediated transcriptional repression of most PCM genes under cold stress.

We determined that mutations in *TOP6A3* and *TOP6B* resulted in higher Chl contents (Chl *a* and Chl *b*) compared with WT seedlings (Figure 1G; Supplementary Data S1). The contents of Chl intermediates (ALA, Mg-protoIX and Chlide) were also significantly increased in the leaves of both mutants relative to the WT (Figure 1G). Although we observed no significant difference in Chl contents in the double overexpressing line under normal growth conditions (Supplementary Figure S1J), we did notice a modest delay in de-etiolation, as evidenced by a delay in leaf greening and Chl accumulation (Supplementary Figure S1H, K), relative to the WT. These phenotypes suggest that *TOP6* genes repress Chl biosynthesis and restrict the accumulation of its biosynthetic intermediates. In agreement with these observations, we also assessed 19 functional genes involved in Chl biosynthesis and revealed that three genes (*HEMA*, *HEMB* and *PORA*) were selectively up-regulated in the leaves of *top6a3* and *top6b* mutant seedlings compared with the WT (Supplementary Figure S2B).

RNA-seq analysis of leaves from the *top6a3* mutant (Figure 2A, B) uncovered 16 up-regulated PCM genes and a set of weakly down-regulated PCM genes, suggesting that TOP6A3 might regulate the two groups of genes differentially under normal temperature conditions. A ChIP-qPCR conducted with an anti-TOP6A3 antibody indicated that

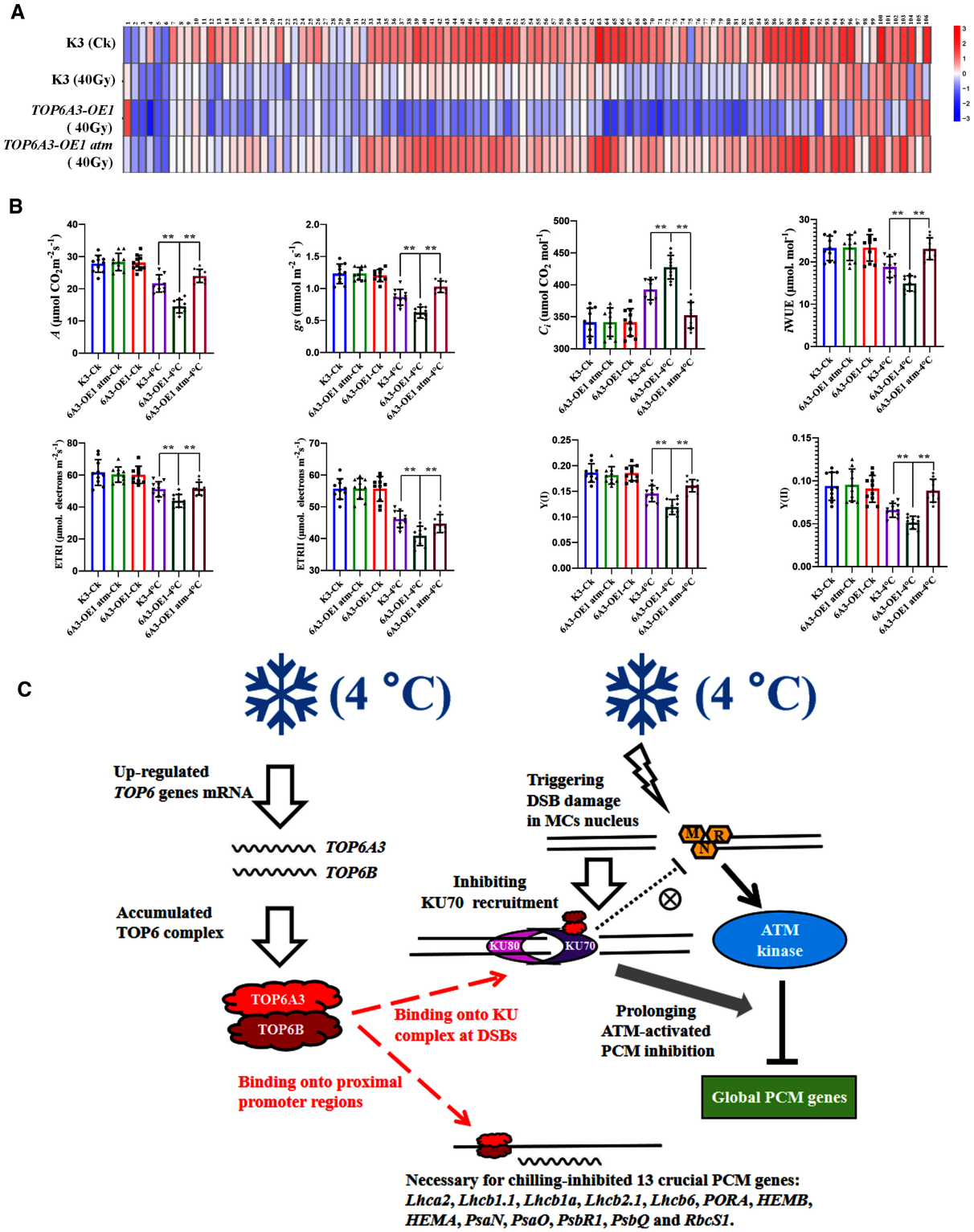

Figure 9. Heatmap representation of the expression of global PCM genes in irradiated WT (K3), *TOP6A3-OE1* and *TOP6A3-OE1 atm* seedlings and measurements of photosynthetic parameters. (**A**) Heatmap representation of 106 PCM genes in K3 seedlings in control conditions and in irradiated K3, *TOP6A3-OE1* and *TOP6A3-OE1 atm* seedlings ($n = 3$). Rice leaves were collected after 6 h of exposure to 40 Gy of γ-irradiation. The full IDs of the PCM genes used in the heatmap are given in Supplementary Table S6. The heatmaps are based on FPKM values of all samples. Blue, low expression; red, high expression. (**B**) Measurements of the photosynthetic parameters in the leaves of K3, *TOP6A3-OE1* and *TOP6A3-OE1 atm* seedlings under control growth conditions or cold stress. *6A3-OE1*, overexpressing line *TOP6A3-OE1*. **Significant difference, *P*-value <0.05, as calculated by one-way ANOVA. (**C**) A simplified mechanistic model displaying the crucial roles fulfilled by the TOP6 complex in integrating cold-repressed PCM genes in rice leaves. MRN, MRN complex. Positive effects are shown by arrows; repressions are depicted by lines ending blunt ends. '⊗' indicates that the DSB–TOP6 complex does not influence the MRN signal.

TOP6A3 bound to the proximal promoter region of 13 up-regulated PCM genes (*Lhca2*, *Lhcb1.1*, *Lhcb1a*, *Lhcb2.1*, *Lhcb6*, *PORA*, *HEMB*, *HEMA*, *PsaN*, *PsaO*, *PsbR1*, *PsbQ* and *RbcS1*) in *TOP6A3-OE1* seedlings and cold-treated K3 seedlings (Figure 2D). Notably, TOP6A3 was also enriched at the promoter regions of two down-regulated genes (*PsbS* and *FD2*), but not at the promoter of genes whose expression was not affected in the *top6a3* mutant (*Lhcb4*, *PS1-F* and *PsbX*) (Figure 2D). Following cold stress, the transcript levels of the 13 up-regulated TOP6A3-bound genes sharply decreased in K3 seedlings, while the expression of the same genes was only modestly repressed in cold-treated mutant seedlings (Figure 2C). These results suggest that the TOP6 complex is indispensable for the transcriptional inhibition of 13 PCM genes during the cold response.

Based on seedling height, we observed that the *TOP6A3-OE1* and *TOP6B-OE1* overexpressing lines were more sensitive to genotoxic drugs than the WT (Figure 3D, E). Strikingly, the *ku70* and *lig4* mutants exhibited a higher BLM sensitivity than the overexpressing lines (Figure 3F, G). We also performed immunofluorescence-based detection of key DSB repair factors in the nuclei of root tip cells in γ-irradiated *TOPA3-OE1 TOP6B-OE1* seedlings, which revealed a specific decrease in foci for LIG4, the last step ligase of the c-NHEJ pathway, in the double overexpressing line relative to the WT (Figure 4E, F). We thus hypothesized that the overexpression of *TOP6* genes led to a reduction in the loading of c-NHEJ pathway components, possibly explaining the hypersensitivity seen in response to genotoxic stress. The COM1 signals in irradiated *TOPA3-OE1 TOP6B-OE1* seedlings were reminiscent of our previous report (31), in which we showed that rice MEIOTIC RECOMBINATION 11 (MRE11) is essential for the loading of COM1 to mediate the alt-NHEJ repair pathway; in addition, the COM1 signal was compromised in irradiated rice seedlings treated with wortmannin, an inhibitor of phosphoinositide 3-kinases. Combined with this study, we suggest that the Mre11–Rad50–Nbs1 (MRN) pathway, which integrates ATM signals and COM1 loading, is working normally in *TOPA3-OE1 TOP6B-OE1* seedlings during the DSB damage response.

The eukaryotic homolog of archaeal Top6A is SPO11, which can induce meiotic DSBs that are subsequently processed by the HR pathway (22,23). In this study, we detected strong TOP6A3 foci in the nuclei of somatic cells from irradiated *TOPA3-OE1 TOP6B-OE1* seedlings (Figure 3C; Supplementary Data S6a). A Y2H assay showed that TOP6A3 and TOP6A3 can form both homodimers and heterodimers (Supplementary Figure S4). We therefore propose that the TOP6 complex is recruited to DSB sites in irradiated *TOPA3-OE1 TOP6B-OE1* seedlings. Moreover, we determined that TOP6A3 specifically interacted with KU70, but not KU80 (Figure 4A, B, D). Competitive EMSAs suggested that TOP6A3 diminished the binding capacity of KU70 to DSB terminals via the TOP6A3–KU70 interaction rather than competitive binding to DSB sites (Figure 4C), and TOP6B appeared to positively contribute to TOP6A3-mediated inhibition of KU70 loading. Together, we propose that TOP6A3 and TOP6B form a complex in the nucleus, after which they bind to KU70 to inhibit its binding at DSB sites, thus repressing the KU-mediated c-NHEJ pathway in *TOP6*-overexpressing lines. In the future, TOP6A3 can be used as an inhibitor against the KU70 loading at DSB terminals in *in vitro* biochemical analysis.

The RNA-seq analysis conducted in this study revealed that γ-irradiation rapidly repressed the expression of PCM pathway genes in rice leaves from WT seedlings (Figure 7A) and in irradiated *atr* mutant seedlings, but not in irradiated *atm-1* seedlings. Indeed, PCM genes remained highly expressed even following IR treatments (Figure 8A), with only two PCM genes being down-regulated (Figure 8B). This result indicated that the repression of PCM gene expression in response to γ-irradiation is largely dependent on the ATM kinase, but not on ATR. A previous report showed that ATM can repress the expression of senescence-associated genes via modulation of histone lysine methylation on the key TF genes (WRKY and NAC family members) in Arabidopsis (65). We speculate that ATM suppresses the expression of photosynthetic genes through epigenetic control of key TF genes whose encoded proteins bind to the promoter regions of PCM-related genes. After a 6 h recovery period from γ-irradiation, we observed a more severe repression of the expression of PCM-related genes in the *ku70* mutant relative to its WT (Supplementary Figure S6), and in irradiated *TOP6A3-OE1* seedlings, although not to the same extent as the *ku70* mutant (Figure 9A). This observation is consistent with the higher susceptibility of the *ku70* mutant to BLM treatment than *TOP6*-overexpressing lines (Figure 3F, G). Thus, we propose that overexpressing *TOP6* genes prolongs the transcriptional repression of PCM genes in irradiated rice leaves by attenuating the efficiency of the c-NHEJ repair.

We observed that rice MCs are prone to DSB damage under cold stress, as evidenced by γ-H2AX immunostaining and comet assays (Figure 5). We hypothesize that the transcriptional repression of PCM genes in response to DSB damage is activated in MCs exposed to cold stress. Indeed, 82 PCM genes were down-regulated in cold-treated WT seedlings, but this effect was greatly reduced in the *atm-1* mutant, with only 18 significantly down-regulated PCM genes (Figure 8C). This observation suggested that ATM also plays an inhibitory role for most PCM genes during the cold response (Figure 8A, C) and that the ATM pathway coordinates the cold stress response and the PCM pathway. Based on the lower γ-H2AX signals in cold-treated MCs from both *top6* mutants (Figure 5B, E) and the higher LIG4 signals in the *top6a3* mutant compared with the WT (Figure 6B, D), we speculate that the inhibition of DSB repair efficiency by cold in rice MCs is mediated by the induction of the TOP6 complex, which subsequently inhibits KU70 binding to cold-induced DSBs and decreases the loading of LIG4 (Figure 9C).

Arabidopsis SPLICING FACTOR 1 (SF1) regulates intron splicing efficiency, which is important in chloroplast development and helps plants acclimate to cold (66). Mutations in rice pentatricopeptide repeat (PPR) proteins, such as WHITE STRIPE LEAF5 (WSL5) and DULAR1 (DUA1), lead to cold-dependent chlorosis (67,68). These reports suggested that plastid translational activity is important for chloroplast development under cold stress conditions. We report here that the transcriptional repression of PCM genes in response to cold is governed by the TOP6–ATM module in rice and is biologically relevant, based

on a series of photosynthetic parameters. Indeed, A_{sat}, g_s, *i*WUE and ETRs were all lower in the *TOP6A3-OE1*-overexpressing line compared with the WT (Figure 9B). Surprisingly, these parameters were normal in *TOP6A3-OE1 atm* seedlings (Figure 9B), suggesting that *ATM* acts downstream of *TOP6A3*.

In summary, we report here a novel role for Spo11/Top6A homologs as c-NHEJ inhibitors in cold-stressed rice seedlings. We proposed that the TOP6 complex acts as an integrator for the cold-mediated repression of PCM gene expression in MCs, via two regulatory functions. We further demonstrated that the inhibition of photosynthesis by cold treatment is controlled by the ATM-activated DSB damage response.

DATA AVAILABILITY

The transcriptome data were deposited at the NCBI under accession number GSE201978 (https://www.ncbi.nlm.nih.gov/geo/query/acc.cgi?acc).

SUPPLEMENTARY DATA

Supplementary Data are available at NAR Online.

ACKNOWLEDGEMENTS

We acknowledge support from Orizymes Biotechnologies (Shanghai) Co., Ltd, for providing techniques/skills for protein experiments. We offer special thanks to Chao Zhang (Yangzhou University, Jiangsu province, China) for sharing the rice mutants (*atm-1* and *atr*) and to Professor Hualing Mi (CAS Center for Excellence in Molecular Plant Science, Shanghai, China) for critical discussions.

Author contributions: Z.X.: conceptualization, methodology, software, investigation, data curation, visualization, writing—original draft preparation, writing—reviewing and editing. J.Z., X.W.: methodology. J.E.: methodology, validation. J.J.: data curation. W.C., Y.X., M.Q.: supervision, validation. All authors read and approved the final manuscript version.

FUNDING

Key-Area Research and Development Program of Guangdong Province [2021B0707010006]; Agricultural funds of Guangzhou City [20101289]; Guangzhou Science and Technology Project [202103000083]; National Natural Science Foundation of China [32170245 and 32260447]; the project of Sanya Yazhou Bay Science and Technology City [SCKJ-JYRC-2022–04]; and Hainan Yazhou Bay Seed Laboratory [B22E1001P].

Conflict of interest statement. The authors declare that they have no conflict of interest concerning this study.

REFERENCES

1. Wagner,D. (1996) Scenarios of extreme temperature events. *Clim. Change*, **33**, 385–407.
2. Tebaldi,C., Hayhoe,K., Arblaster,J.M. and Meehl,G.A. (2006) Going to the extremes: an intercomparison of model-simulated historical and future changes in extreme events. *Clim. Change*, **79**, 185–211.
3. Zhu,J., Dong,C.H. and Zhu,J.K. (2007) Interplay between cold-responsive gene regulation, metabolism and RNA processing during plant cold acclimation. *Curr. Opin. Plant Biol.*, **10**, 290–295.
4. Ma,Y., Dai,X., Xu,Y., Luo,W., Zheng,X., Zeng,D., Pan,Y., Lin,X., Liu,H., Zhang,D. *et al.* (2015) COLD1 confers chilling tolerance in rice. *Cell*, **160**, 1209–1221.
5. Sage,R.F. and Kubien,D.S. (2007). The temperature response of C3 and C4 photosynthesis. *Plant Cell Environ.*, **30**, 1086–1106.
6. Yamori,W., Hikosaka,K. and Way,D.A. (2014) Temperature response of photosynthesis in C3, C4, and CAM plants: temperature acclimation and temperature adaptation. *Photosynth. Res.*, **119**, 101–117.
7. Berry,J.A. and Bjo¨rkman,O. (1980) Photosynthetic response and adaptation to temperature in higher plants. *Annu. Rev. Plant Physiol.*, **31**, 491–543
8. Allen,D.J. and Ort,D.R. (2001) Impacts of chilling temperatures on photosynthesis in warm-climate plants. *Trends Plant Sci.*, **6**, 36–42.
9. Hikosaka,K., Ishikawa,K., Borjigidai,A., Muller,O. and Onoda,Y. (2006) Temperature acclimation of photosynthesis: mechanisms involved in the changes in temperature dependence of photosynthetic rate. *J. Exp. Bot.*, **57**, 291–302.
10. Liu,X., Lan,J., Huang,Y., Cao,P., Zhou,C., Ren,Y., He,N., Liu,S., Tian,Y., Nguyen,T. *et al.* (2018) WSL5, a pentatricopeptide repeat protein, is essential for chloroplast biogenesis in rice under cold stress. *J. Exp. Bot.*, **69**, 3949–3961.
11. Chaves,M.M., Flexas,J. and Pinheiro,C. (2009) Photosynthesis under drought and salt stress: regulation mechanisms from whole plant to cell. *Ann. Bot.*, **103**, 551−60.
12. Ambavaram,M.M., Basu,S., Krishnan,A., Ramegowda,V., Batlang,U., Rahman,L., Baisakh,N. and Pereira,A. (2014) Coordinated regulation of photosynthesis in rice increases yield and tolerance to environmental stress. *Nat. Commun.*, **5**, 5302.
13. Zhang,Q., Chen,Q., Wang,S., Hong,Y. and Wang,Z. (2014) Rice and cold stress: methods for its evaluation and summary of cold tolerance-related quantitative trait loci. *Rice*, **7**, 24.
14. Zhang,T., Zhao,X., Wang,W., Pan,Y., Huang,L., Liu,X., Zong,Y., Zhu,L., Yang,D. and Fu,B. (2012) Comparative transcriptome profiling of chilling stress responsiveness in two contrasting rice genotypes. *PLoS One*, **7**, e43274.
15. Pradhan,S.K., Pandit,E., Nayak,D.K., Behera,L. and Mohapatra,T. (2019) Genes, pathways and transcription factors involved in seedling stage chilling stress tolerance in indica rice through RNA-Seq analysis. *BMC Plant Biol.*, **19**, 352.
16. Wu.,H-Y. and Liu,L.F. (1991) DNA looping alters local DNA conformation during transcription. *J. Mol. Biol.*, **219**, 615–622.
17. Kretzschmar,M., Meisterernst.,M. and Roeder,R.G. (1993) Identification of human DNA topoisomerase I as a cofactor for activator-dependent transcription by RNA polymerase II. *Proc. Natl Acad. Sci. USA*, **90**, 11508–11512.
18. Merino,A., Madden,K.R., Lane,W.S., Champoux,J.J. and Reinberg.,D. (1993) DNA topoisomerase I is involved in both repression and activation of transcription. *Nature*, **365**, 227–232.
19. D'Arpa,P., Beardmore,C. and Liu,L.F. (1990) Involvement of nucleic acid synthesis in cell killing mechanisms of topoisomerase poisons. *Cancer Res.*, **50**, 6919−6924.
20. Theilmann,H.W., Popanda,O., Gersbach,H. and Gilberg,F. (1993) Various inhibitors of DNA topoisomerases diminish repair-specific DNA incision in UV-irradiated human fibroblasts. *Carcinogenesis*, **14**, 2341–2351.
21. Ashour,M.E., Atteya,R. and El-Khamisy,S.F. (2015) Topoisomerase-mediated chromosomal break repair: an emerging player in many games. *Nat. Rev. Cancer*, **15**, 137–151.
22. Bergerat,A., Gadelle,D. and Forterre,P. (1994) Purification of a DNA topoisomerase II from the hyperthermophilic archaeon *Sulfolobus shibatae*. A thermostable enzyme with both bacterial and eucaryal features. *J. Biol. Chem.*, **269**, 27663–27669.
23. Buhler,C., Gadelle,D., Forterre,P., Wang,J.C. and Bergerat,A. (1998) Reconstitution of DNA topoisomerase VI of the thermophilic archaeon *Sulfolobus shibatae* from subunits separately overexpressed in *Escherichia coli*. *Nucleic Acids Res.*, **26**, 5157–5162.
24. Keeney,S., Giroux,C.N. and Kleckner,N. (1997) Meiosis-specific DNA double-strand breaks are catalyzed by Spo11, a member of a widely conserved protein family. *Cell*, **88**, 375–384.
25. Keeney,S. and Neale,M.J. (2006) Initiation of meiotic recombination by formation of DNA double-strand breaks: mechanism and regulation. *Biochem. Soc. Trans.*, **34**, 523–525.
26. Stacey,N.J., Kuromori,T., Azumi,Y., Roberts,G., Breuer,C., Wada,T., Maxwell,A., Roberts,K. and Sugimoto-Shirasu,K. (2006)

Arabidopsis SPO11-2 functions with SPO11-1 in meiotic recombination. *Plant J.*, **48**, 206–216.
27. Sugimoto-Shirasu,K., Stacey,N.J., Corsar,J., Roberts,K. and McCann,M.C. (2002) DNA topoisomerase VI is essential for endoreduplication in Arabidopsis. *Curr. Biol.*, **12**, 1782–1786.
28. Yin,Y., Cheong,H., Friedrichsen,D., Zhao,Y., Hu,J., Mora-Garcia,S. and Chory,J. (2002) A crucial role for the putative Arabidopsis topoisomerase VI in plant growth and development. *Proc. Natl Acad. Sci. USA*, **99**, 10191–10196.
29. Gilkerson,J. and Callis,J. (2014) A genetic screen for mutants defective in IAA1-LUC degradation in *Arabidopsis thaliana* reveals an important requirement for *TOPOISOMERASE6B* in auxin physiology. *Plant Signal. Behav.*, **9**, e972207.
30. Simková,K., Moreau,F., Pawlak,P., Vriet,C., Baruah,A., Alexandre,C., Hennig,L., Apel,K. and Laloi,C. (2012) Integration of stress-related and reactive oxygen species-mediated signals by topoisomerase VI in *Arabidopsis thaliana*. *Proc. Natl Acad. Sci. USA*, **109**, 16360–16365.
31. Xu,Z., Zhang,J., Cheng,X., Tang,Y., Gong,Z., Gu,M. and Yu,H. (2020) COM1, a factor of alternative non-homologous end joining, lagging behind the classic non-homologous end joining pathway in rice somatic cells. *Plant J.*, **103**, 140–153.
32. Zhang,C., Zhang,F., Cheng,X., Liu,K., Tang,J., Li,Y., Tang,D., Cheng,Z. and Yu,H. (2020) OsATM safeguards accurate repair of meiotic double-strand breaks in rice. *Plant Physiol.*, **183**, 1047–1057.
33. Shan,Q., Wang,Y., Li,J., Zhang,Y., Chen,K., Liang,Z., Zhang,K., Liu,J., Xi,J.J., Qiu,J.L. *et al.* (2013) Targeted genome modification of crop plants using a CRISPR-Cas system. *Nat. Biotechnol.*, **31**, 686–688.
34. Qu,M., Hamdani,S., Li,W., Wang,S., Tang,J., Chen,Z., Song,Q., Li,M., Zhao,H., Chang,T. *et al.* (2016) Rapid stomatal response to fluctuating light: an under-explored mechanism to improve drought tolerance in rice. *Funct. Plant Biol.*, **43**, 727–738.
35. Livak,K.J. and Schmittgen,T.D. (2001) Analysisof relative gene expression data using real-time quantitative PCR and the $2^{-\Delta\Delta CT}$ method. *Methods*, **25**, 402–408.
36. Wang,K., Tang,D., Wang,M., Lu,J., Yu,H., Liu,J., Qian,B., Gong,Z., Wang,X., Chen,J. *et al.* (2009) MER3 is required for normal meiotic crossover formation, but not for presynaptic alignment in rice. *J. Cell Sci.*, **122**, 2055–2063.
37. Wang,H., Hu,Q., Tang,D., Liu,X., Du,G., Shen,Y., Li,Y. and Cheng,Z. (2016) OsDMC1 is not required for homologous pairing in rice meiosis. *Plant Physiol.*, **171**, 230–241.
38. Chen,H., Zou,Y., Shang,Y., Lin,H., Wang,Y., Cai,R., Tang,X. and Zhou,J.M. (2008) Firefly luciferase complementation imaging assay for protein–protein interactions in plants. *Plant Physiol.*, **146**, 368–376.
39. Bowler,C., Benvenuto,G., Laflamme,P., Molino,D., Probst,A.V., Tariq,M. and Paszkowski,J. (2004) Chromatin techniques for plant cells. *Plant J.*, **39**, 776–789.
40. Liu,C.T., Wu,Y.B. and Wang,X.P. (2012) bZIP transcription factor OsbZIP52/RISBZ5: a potential negative regulator of cold and drought stress response in rice. *Planta*, **235**, 1157–1169.
41. Zhang,W., Lee,H.R., Koo,D.H. and Jiang,J.M. (2008) Epigenetic modification of centromeric chromatin: hypomethylation of DNA sequences in the CENH3-associated chromatin in *Arabidopsis thaliana* and maize. *Plant Cell*, **20**, 25–34.
42. Kwon,Y.I., Abe,K., Endo,M., Osakabe,K., Ohtsuki,N., Nishizawa-Yokoi,A., Tagiri,A., Saika,H. and Toki,S. (2013) DNA replication arrest leads to enhanced homologous recombination and cell death in meristems of rice OsRecQl4 mutants. *BMC Plant Biol.*, **13**, 62.
43. Yan,Z.Y., Chen,J., Shao,J., Jiao,Z.Q., Tang,T.S., Tang,M., Sheng,Z.G., Mao,L., Huang,R., Huang,C.H. *et al.* (2021) The cell-impermeable Ru(II) polypyridyl complex as a potent intracellular photosensitizer under visible light irradiation via ion-pairing with suitable lipophilic counter-anions. *Free Radic. Biol. Med.*, **171**, 69–79.
44. Hartung,F. and Puchta,H. (2001) Molecular characterization of homologues of both subunits A (SPO11) and B of the archaebacterial topoisomerase 6 in plants. *Gene*, **271**, 81–86.
45. Zhao,Y., Han,Q., Ding,C., Huang,Y., Liao,J., Chen,T., Feng,S., Zhou,L., Zhang,Z., Chen,Y. *et al.* (2020) Effect of low temperature on chlorophyll biosynthesis and chloroplast biogenesis of rice seedlings during greening. *Int. J. Mol. Sci.*, **21**, 1390.
46. Nitiss,J.L. and Wang,J.C. (1996) Mechanisms of cell killing by drugs that trap covalent complexes between DNA topoisomerases and DNA. *Mol. Pharmacol.*, **50**, 1095–1102.
47. Pommier,Y., Barcelo,J.M., Rao,V.A., Sordet,O., Jobson,A.G., Thibaut,L., Miao,Z.H., Seiler,J.A., Zhang,H., Marchand,C. *et al.* (2006) Repair of topoisomerase I-mediated DNA damage. *Prog. Nucleic Acid Res. Mol. Biol.* **81**, 179–229.
48. Xu,Z., Zhang,J., Xu,M., Ji,W., Yu,M., Tao,Y., Gong,Z., Gu,M. and Yu,H. (2018) Rice RAD51 paralogs play essential roles in somatic homologous recombination for DNA repair. *Plant J.*, **95**, 282–295.
49. Toki,S. (1997) Rapid and efficient Agrobacterium-mediated transformation in rice. *Plant Mol. Biol.*, **15**, 16–21.
50. Kinner,A., Wu,W., Staudt,C. and Iliakis,G. (2008) γ-H2AX in recognition and signaling of DNA double-strand breaks in the context of chromatin. *Nucleic Acids Res.*, **36**, 5678–5694.
51. Amiard,S., Charbonnel,C., Allain,E., Depeiges,A., White,C.I. and Gallego,M.E. (2010) Distinct roles of the ATR kinase and the Mre11–Rad50–Nbs1 complex in the maintenance of chromosomal stability in Arabidopsis. *Plant Cell*, **22**, 3020–3033.
52. Koukalová,B., Kovarík,A., Fajkus,J. and Siroky,J. (1997) Chromatin fragmentation associated with apoptotic changes in tobacco cells exposed to cold stress. *FEBS Lett.*, **414**, 289–292.
53. Ning,S.B., Song,Y.C. and Damme Pv,P.V. (2002) Characterization of the early stages of programmed cell death in maize root cells by using comet assay and the combination of cell electrophoresis with annexin binding. *Electrophoresis*, **23**, 2096–2102.
54. Hong,J.H., Savina,M., Du,J., Devendran,A., Kannivadi Ramakanth,K., Tian,X., Sim,W.S., Mironova,V.V. and Xu,J. (2017) A sacrifice-for-survival mechanism protects root stem cell niche from chilling stress. *Cell*, **170**, 102–113.
55. Kurz,E. and Lees-Miller,S. (2004) DNA damage-induced activation of ATM and ATM-dependent signaling pathways. *DNA Repair (Amst.)*, **3**, 889–900.
56. Shechter,D., Constanzo,V. and Gautier,J. (2004) Regulation of DNA replication by ATR: signaling in response to DNA intermediates. *DNA Repair (Amst.)*, **3**, 901–908.
57. Li,J., Liang,W., Liu,Y., Ren,Z., Ci,D., Chang,J. and Qian,W. (2022) The Arabidopsis ATR–SOG1 signaling module regulates pleiotropic developmental adjustments in response to 3'-blocked DNA repair intermediates. *Plant Cell*, **34**, 852–866.
58. Tanaka,A. and Tanaka,R. (2006) Chlorophyll metabolism. *Curr. Opin. Plant Biol.*, **9**, 248–255.
59. Tamoi,M. and Shigeoka,S. (2015) Diversity of regulatory mechanisms of photosynthetic carbon metabolism in plants and algae. *Biosci. Biotechnol. Biochem.*, **79**, 870–876.
60. Xiong,W., Cano,M., Wang,B., Douchi,D. and Yu,J. (2017) The plasticity of cyanobacterial carbon metabolism. *Curr. Opin. Chem. Biol.*, **41**, 12–19.
61. Kirschbaum,M.U. (2004) Direct and indirect climate change effects on photosynthesis and transpiration. *Plant Biol. (Stuttg).*, **6**, 242–253.
62. Ashraf,M. and Harris,P.C. (2013) Photosynthesis under stressful environments: an overview. *Photosynthetica*, **51**, 163–190.
63. Andaya,V.C. and Mackill,D.J. (2003) Mapping of QTLs associated with cold tolerance during the vegetative stage in rice. *J. Exp. Bot.*, **54**, 2579–2585.
64. Han,Q.H., Huang,B., Ding,C.B., Zhang,Z.W., Chen,Y.E., Hu,C., Zhou,L.J., Huang,Y., Liao,J.Q., Yuan,S. *et al.* (2017) Effects of melatonin on anti-oxidative systems and photosystem II in cold-stressed rice seedlings. *Front. Plant Sci.*, **8**, 785.
65. Li,Z., Kim,J.H., Kim,J., Lyu,J.I., Zhang,Y., Guo,H., Nam,H.G. and Woo,H.R. (2020) ATM suppresses leaf senescence triggered by DNA double-strand break through epigenetic control of senescence-associated genes in Arabidopsis. *New Phytol.*, **227**, 473–484.
66. Zhu,Y., Wu,W., Shao,W., Chen,J., Shi,X., Ma,X., Xu,Y.Z., Huang,W. and Huang,J. (2020) SPLICING FACTOR1 is important in chloroplast development under cold stress. *Plant Physiol.*, **184**, 973–987.
67. Liu,X., Zhou,Y., Xiao,J. and Bao,F. (2018) Effects of chilling on the structure, function and development of chloroplasts. *Front. Plant Sci.*, **9**, 1715.
68. Cui,X., Wang,Y., Wu,J., Han,X., Gu,X., Lu,T. and Zhang,Z. (2019) The RNA editing factor DUA1 is crucial to chloroplast development at low temperature in rice. *New Phytol.*, **221**, 834–849.